USER GUIDE

VERSION 3.0

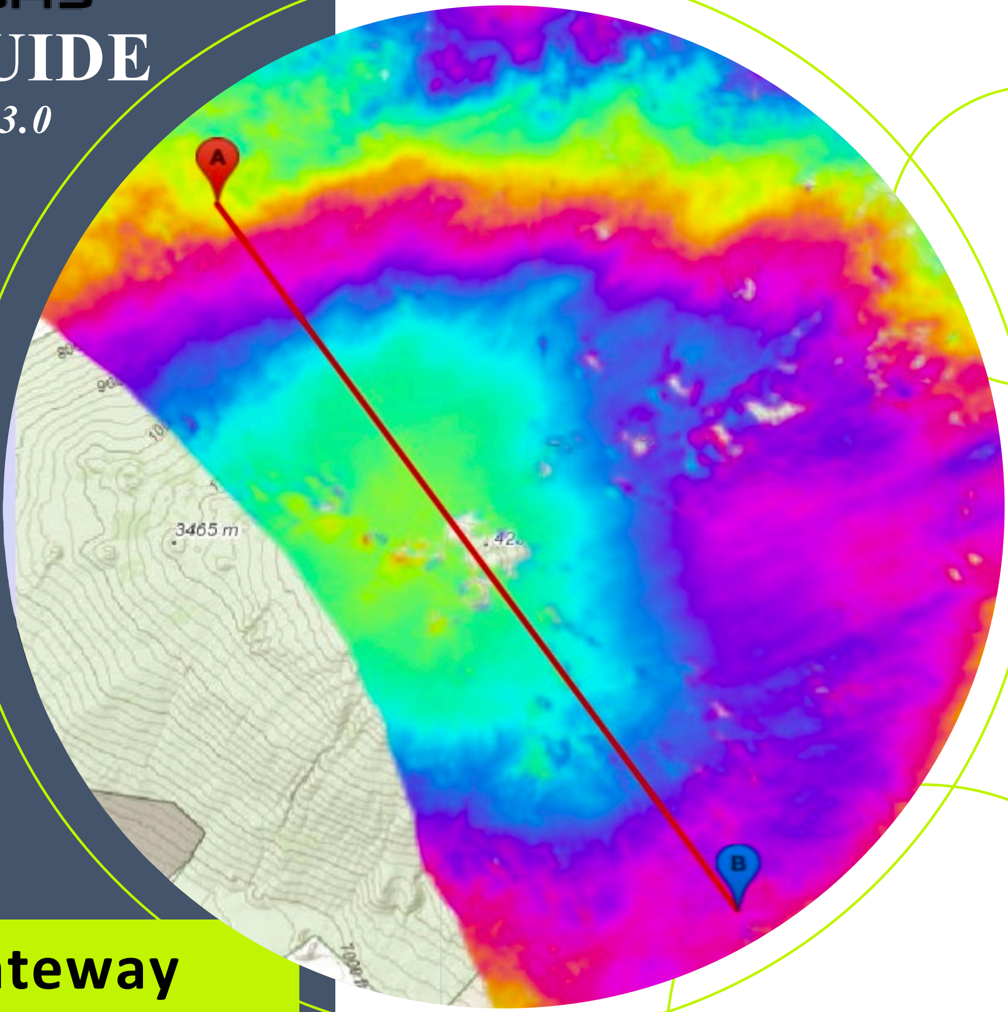

GeoGateway

Tools for **Analysis**, **Modeling**, and Response Using **Geodetic Imaging** and **Global Positioning System** Products.

Government Sponsorship Acknowledgement

Acknowledgments

The User Guide was developed primarily by:

Megan Ani Mirkhanian (mmirkhan@uci.edu), University of California, Irvine
Lisa Grant Ludwig (lgrant@uci.edu), University of California, Irvine

With assistance from other GeoGateway team members:

Andrea Donnellan (andrea.donnellan@jpl.nasa.gov), Jet Propulsion Laboratory
Jay Parker (jay.w.parker@jpl.nasa.gov), Jet Propulsion Laboratory

Other GeoGateway contributing members include:

John Rundle (jbrundle@ucdavis.edu), University of California, Davis
Jun Wang (wang208@iu.edu), Indiana University
Marlon Pierce (marpierc@iu.edu), Indiana University
Yu (Marie) Ma (yuma@iu.edu), Indiana University
Nicholas Mowery (nbmowery@iu.edu), Indiana University
Simran Harshverdhan Mhatre (shmhatre@iu.edu), Indiana University
Robert A Granat (granat@gmail.com), State University of New York
Michael B Heflin (michael.b.heflin@jpl.nasa.gov), Jet Propulsion Laboratory
Margaret T Glasscoe (margaret.t.glasscoe@jpl.nasa.gov), Jet Propulsion Laboratory
Robert Zinke (Robert.zinke@jpl.nasa.gov), Jet Propulsion Laboratory
Nathan Pulver (nathan.pulver@jpl.nasa.gov), Jet Propulsion Laboratory
Gregory Lyzenga (lyzenga@hmc.edu), Harvey Mudd College

Table of Contents

Overview

GeoGateway is a data product search and analysis gateway for scientific discovery, field use, and disaster response.

GeoGateway consists of NASA's geodetic imaging products including InSAR (interferometric synthetic aperture radar) and GNSS (Global Navigation Satellite System), integrated with earthquake faults datasets, seismicity, and models.

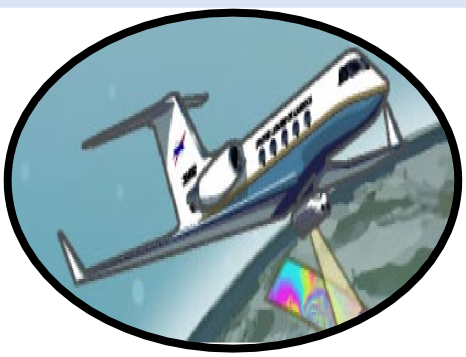

Figure 1: UAVSAR Science Aircraft. (Figure adapted from Jet Propulsion Laboratory (JPL))

The purpose of GeoGateway is to increase the value of existing geodetic imaging products from NASA as well as GNSS products from USGS to enable researchers to explore and integrate these data products.

Goals

- Bridge the gap between production and end-use of data products
- Simplify discovery of geodetic imaging and GNSS data products
- Enable researchers to explore and integrate data products
- Allow researchers to easily share, publish, and collaborate

Figure 2: UAVSAR Science Aircraft. (Figure adapted from Jet Propulsion Laboratory (JPL))

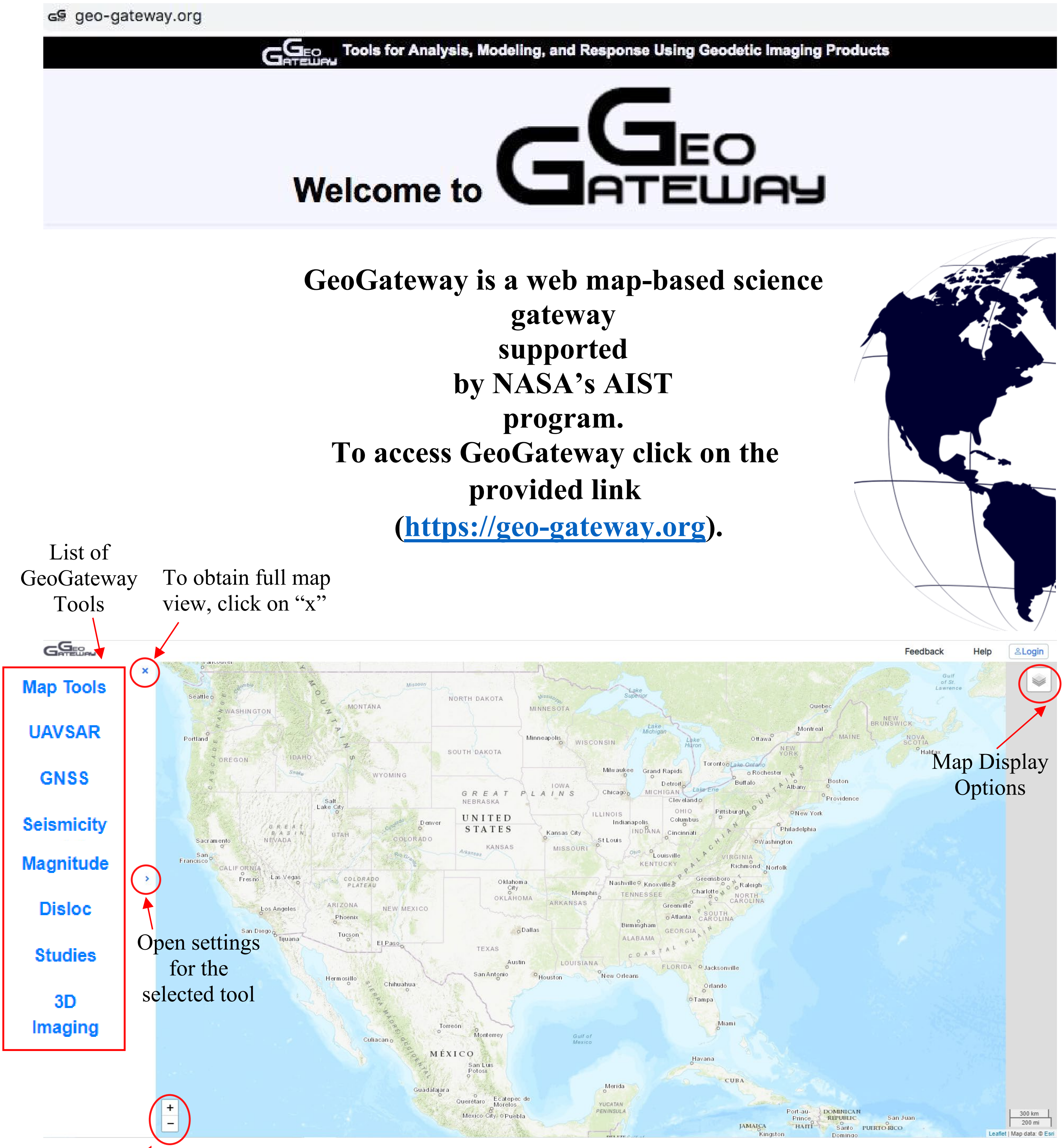

Figure 3: Overview of GeoGateway's tabs

Map Tools

UCERF3 Faults
(Uniform California Earthquake Rupture Forecast, version 3)

The U.S. Geological Survey (USGS) UCERF3 faults (https://pubs.usgs.gov/of/2013/1165/) can be plotted with 4 color options for user preference. To insert the fault lines, check the box next to "UCERF3 Faults." Users are given the option to choose from either black, yellow, red, or grey faults. To obtain more information regarding a particular fault, click on the fault and a popup with information pertaining to the selected fault will appear.

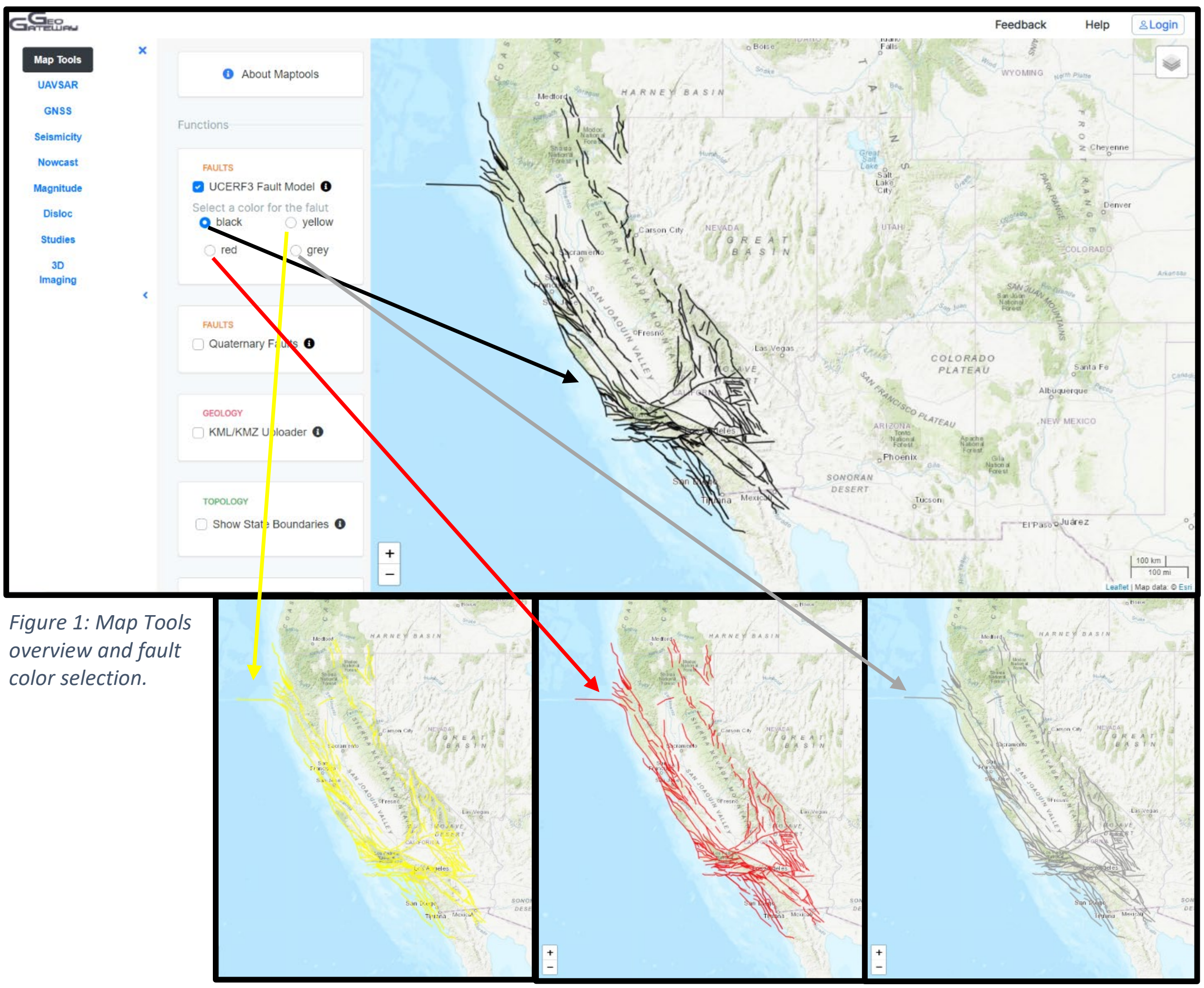

Figure 1: Map Tools overview and fault color selection.

Quaternary Faults

Quaternary faults demonstrate geologic evidence of coseismic surface deformation in the Quaternary (the past 1.6 million years). As shown in *figure 2*, different age Quaternary faults are labeled and colored according to when they last ruptured. Class B faults are either those faults that might not extend deep enough to be considered a possible source for causing earthquakes or there is insufficient geological evidence to be classified in another class. Users may select the Quaternary fault(s) of choice by checking and unchecking the boxes shown under "USGS Faults Database." (Data source: https://doi.org/10.5066/F7S75FJM)

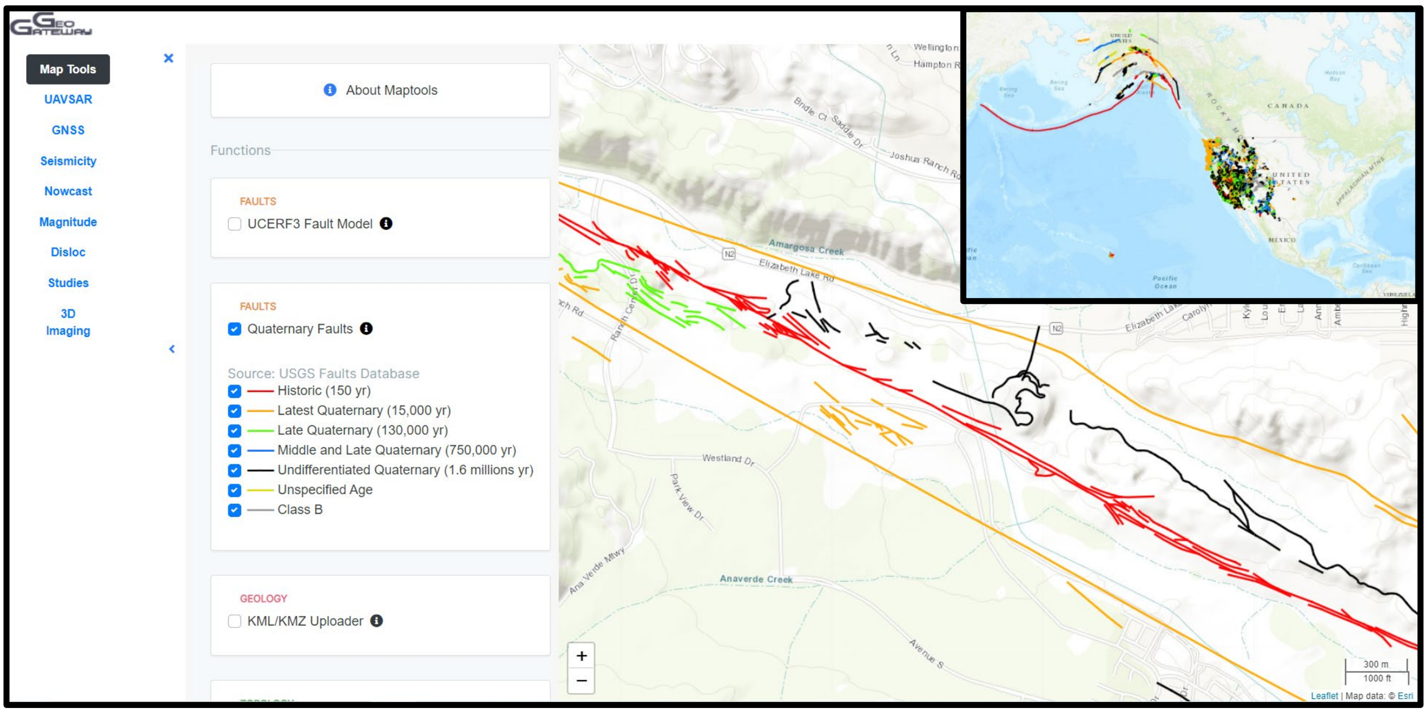

Figure 2: Quaternary faults within Map Tools tab.

KML Uploader

KML (Keyhole Markup Language) is a file format used to display geographic data.
For *example*, visiting the USGS website below,

https://earthquake.usgs.gov/earthquakes/search/

allows for users to search through an earthquake catalog in which the selected earthquake data can be downloaded as a KML file and uploaded into GeoGateway as shown in *figure 3*.
Once uploaded into GeoGateway, the KML file(s) are displayed.

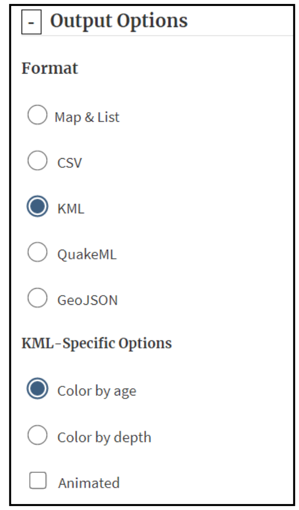

Figure 3: USGS earthquakes catalog output options

By clicking the box next to the uploaded KML file, the file will be displayed on the map.

In this case, the KML file named “USGS_Earthquakes” is displayed on the map.

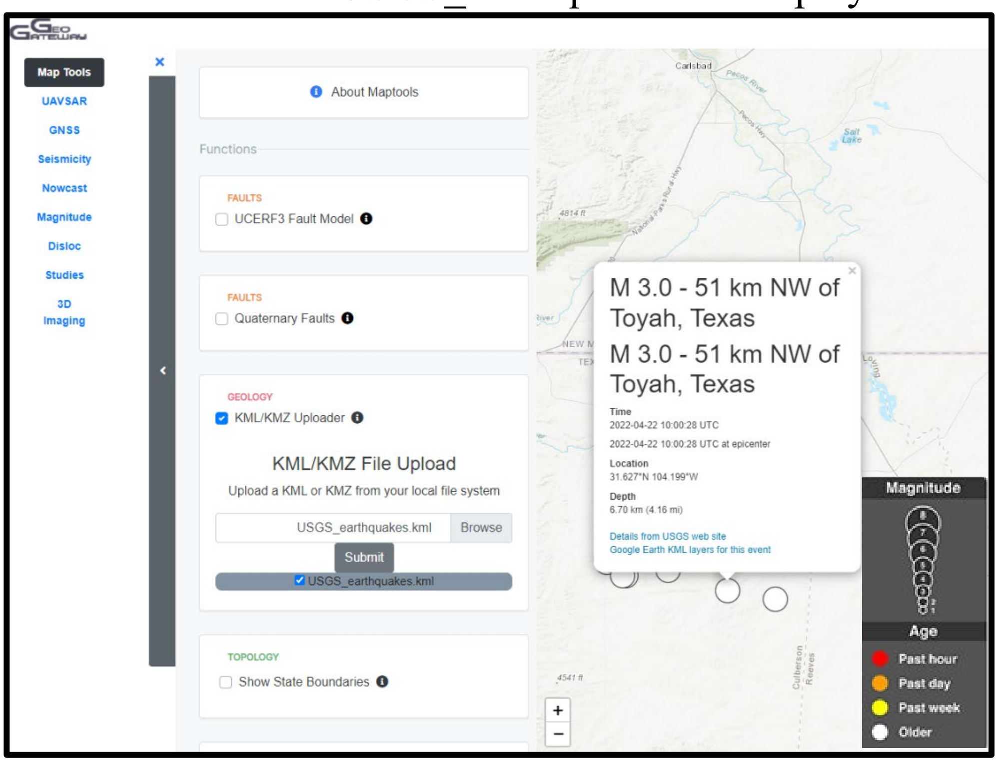

Figure 4: Downloaded KML file from USGS displayed on the map

Show State Boundaries

To display state boundaries within the United States, check the box next to "Show State Boundaries."

Figure 5: Map Tools, United States boundary layer

Show Coastlines

To display coastlines, check the box next to "Show Coastlines."

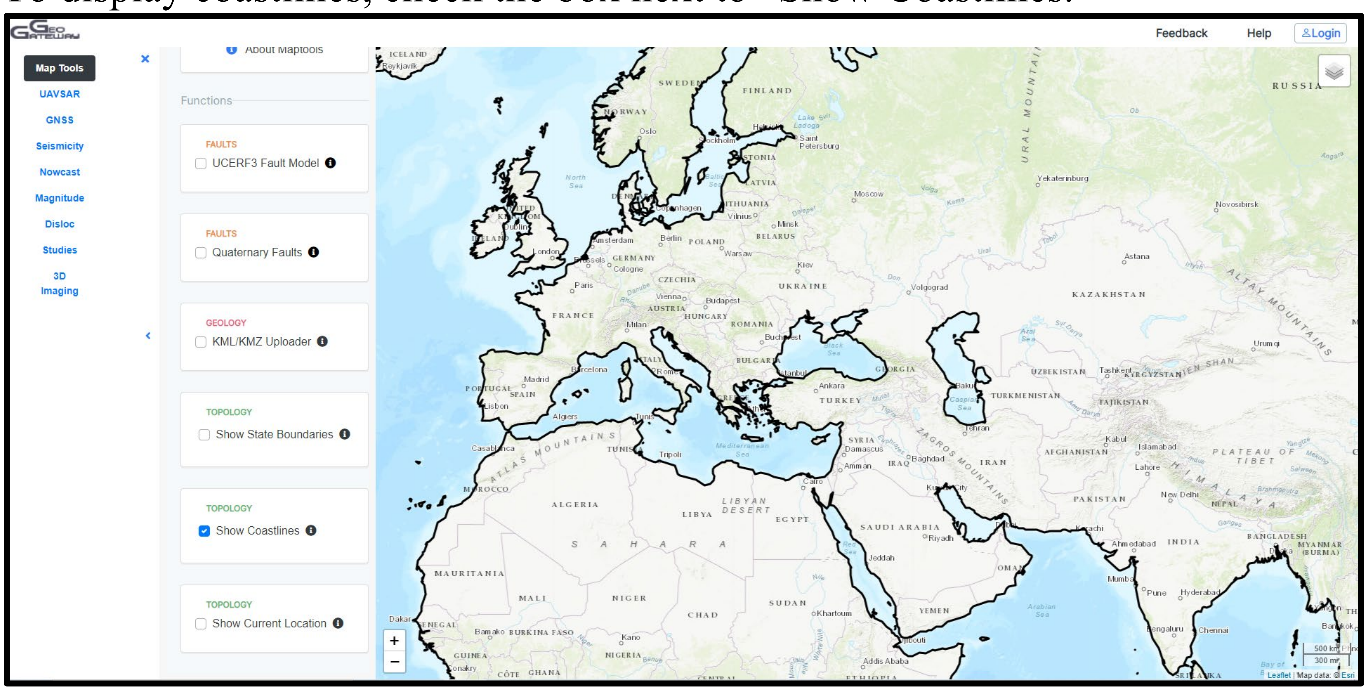

Figure 6: Map Tools, global coastlines layer

Show Current Location

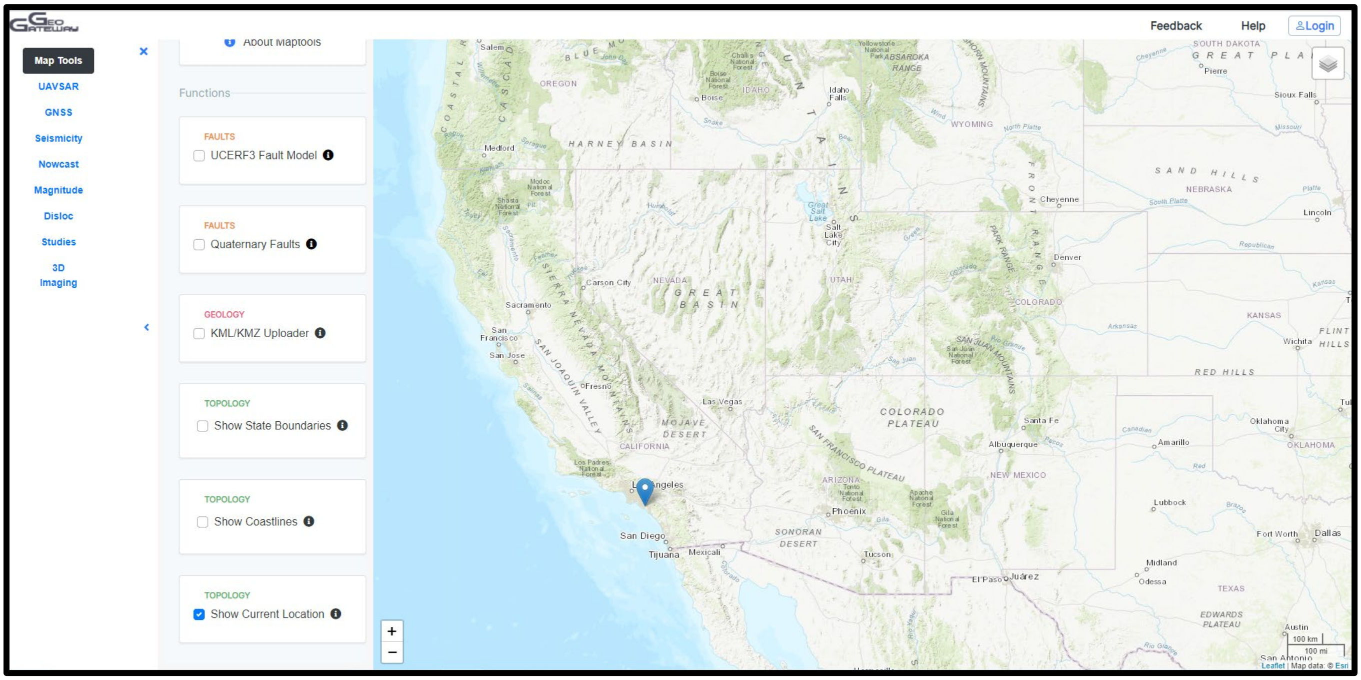

Figure 7: Map Tools, show current location option

By clicking on “Show Current Location” users are able to view their current location on the map.

View map in different modes

By toggling over to right corner, choose either “ArcGIS Topo Map,” “ArcGIS Light Map,” “ArcGIS Dark Map.”

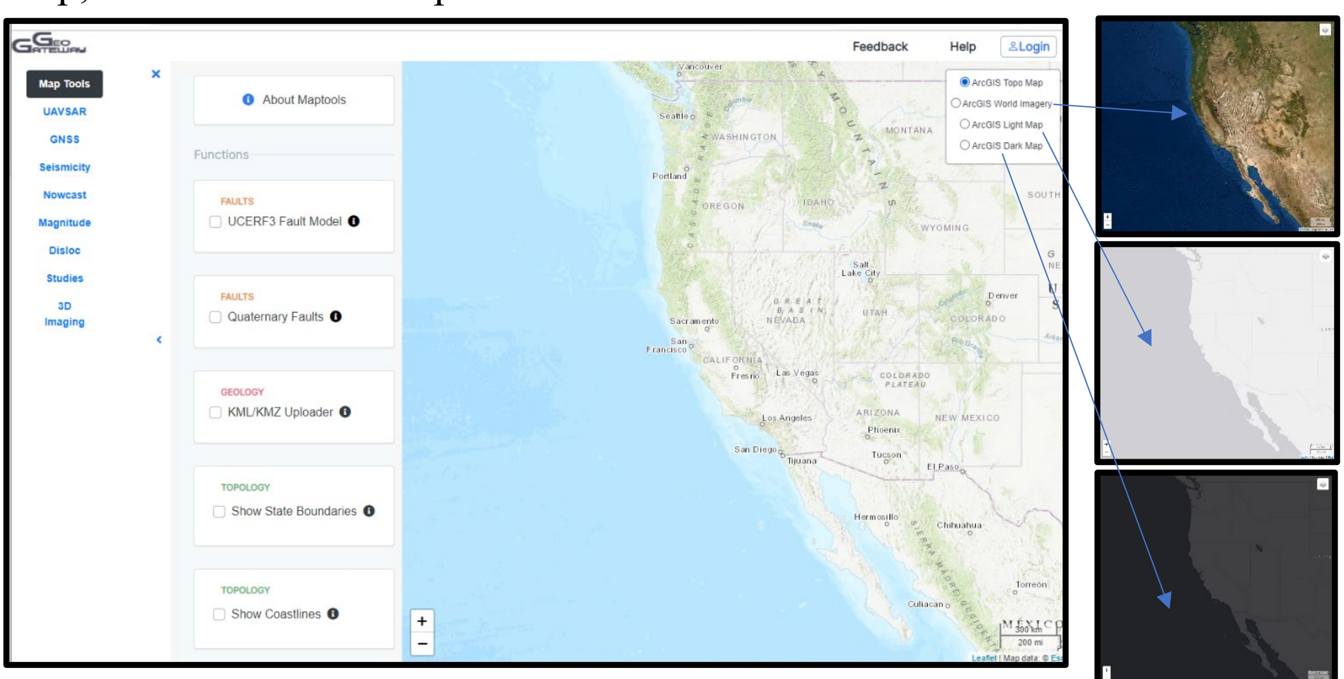

Figure 8: Map Tools, different map coloring options

UAVSAR

UAVSAR (Uninhabited Aerial Vehicle Synthetic Aperture Radar), is an airborne, L-band, fully polarimetric radar, housed in a pod that is mounted to the belly of a piloted Gulfstream III aircraft. Interferometric radar images, or interferograms, are generated from repeat passes flown over a site of interest. Interferometric radar observations are made from the swaths received, which are approximately 22 km wide and typically between 100 and 300 km long (Donnellan et al., 2014).

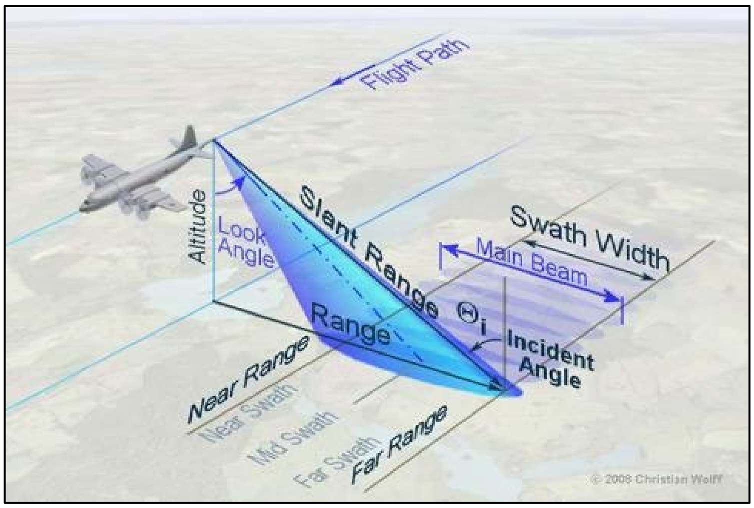

Figure 1: Demonstration of the uninhabited aerial vehicle flight path and how the swath path is determined. (Figure adapted from (Christian Wolff, 2008))

The wide swath of the UAVSAR instrument results in a large incidence angle variation across the swath. Near range incidence angles are approximately 25° whereas far range incidence angles are approximately 65° resulting in a 40° incidence angle variation across the swath.

Since repeat pass radar interferometric measurements only capture the component of surface motion along the line-of-sight vector, it is important to account for imaging geometry variations. Thus, a constant vertical displacement will exhibit a line-of-sight displacement that varies as the cosine of the look angle (angle between aircraft nadir vector and line of sight) and a constant cross-track displacement will exhibit a line-of-sight displacement that varies as the sine of the look angle.

Different fault geometries and types of slip produce different surface motions and project differently onto a line-of-sight change between points on the ground and instrument.

Interpreting line-of-sight changes for fault motions requires assumptions for the style of faulting. Slip of a certain orientation, corresponding to fault slip, can be projected onto line-of-sight between the ground and instrument using the following parameters (Donnellan et al., 2014).

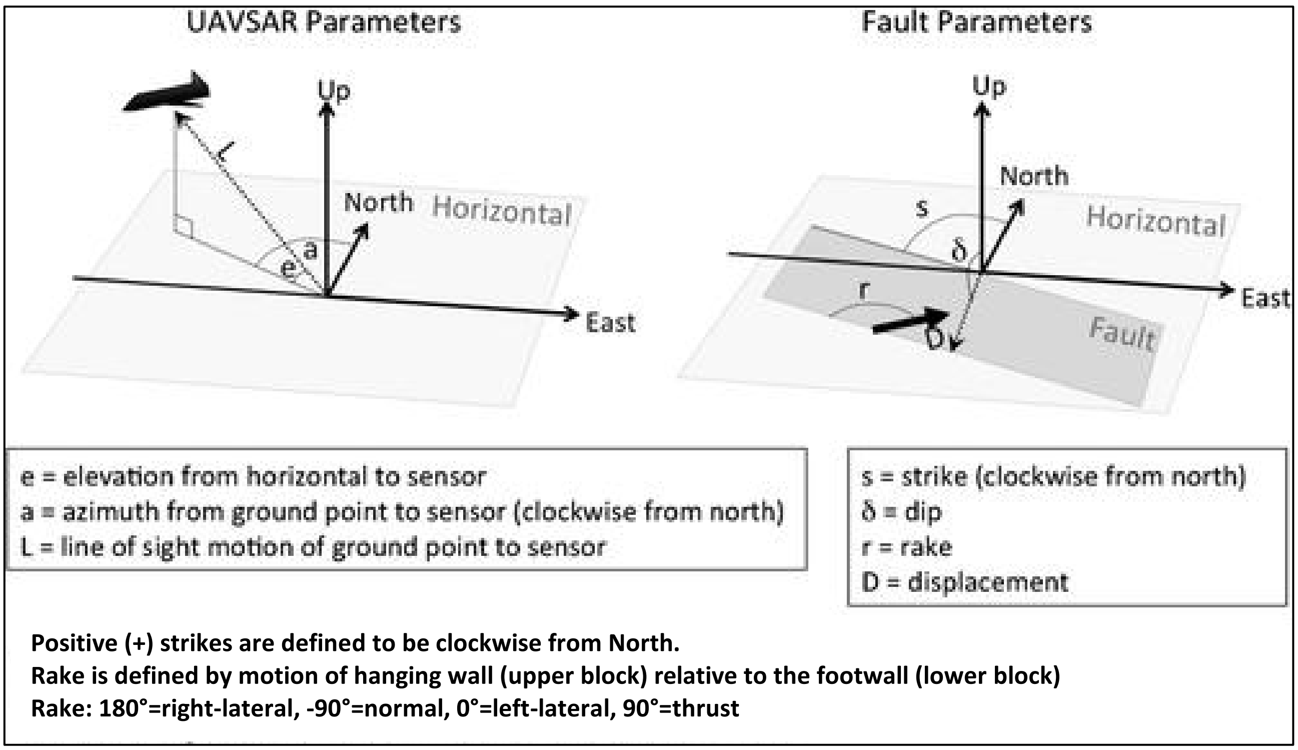

Figure 2: UAVSAR Parameters and Fault Parameters. (Figure adapted from (Donnellan et al., 2014))

To the right, we see two different radar images creating the interferogram (shows the change or difference from each radar image).

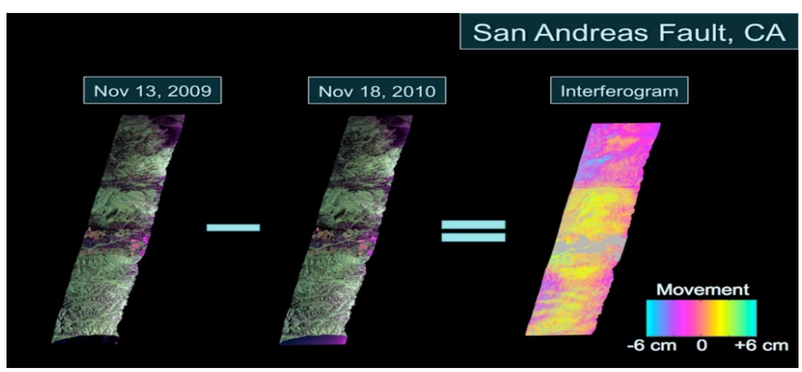

Figure 3: Demonstration the difference between two swaths in the same location on two different dates, which results in an interferogram. (Figure adapted from (Jet Propulsion Laboratory, 2014))

Example UAVSAR uses:

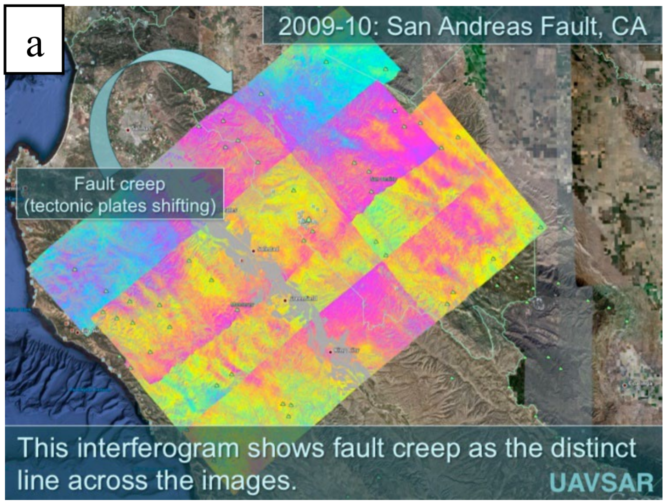

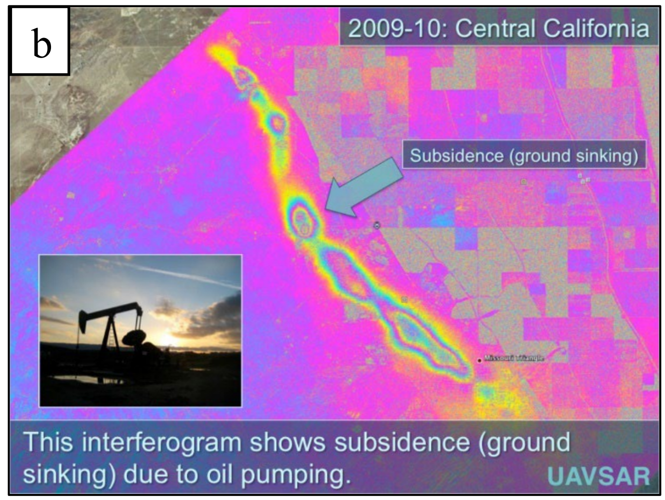

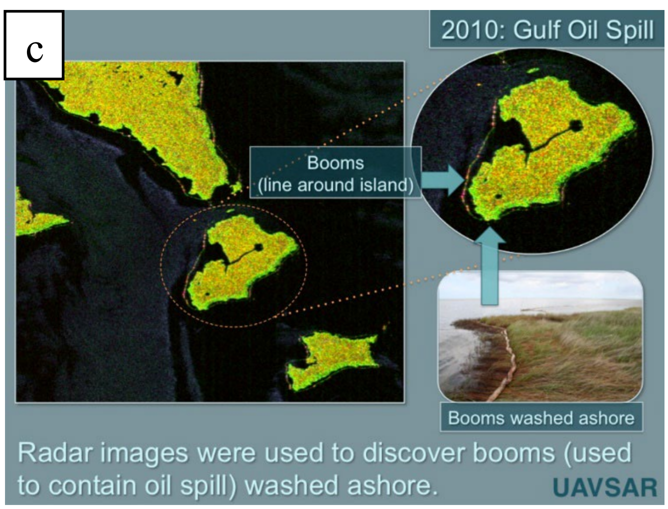

To upload UAVSAR interferograms, follow either method (1) or (2)

1. The “flight name/path” directly finds the flight name and path wanted
2. The “latitude, longitude” option returns all flight swaths crossing paths with those coordinates.

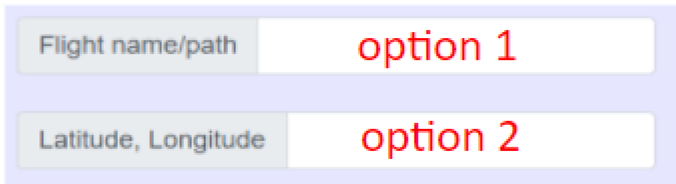

*Note options to draw an area or drop a pin can assist users to finding an interferogram

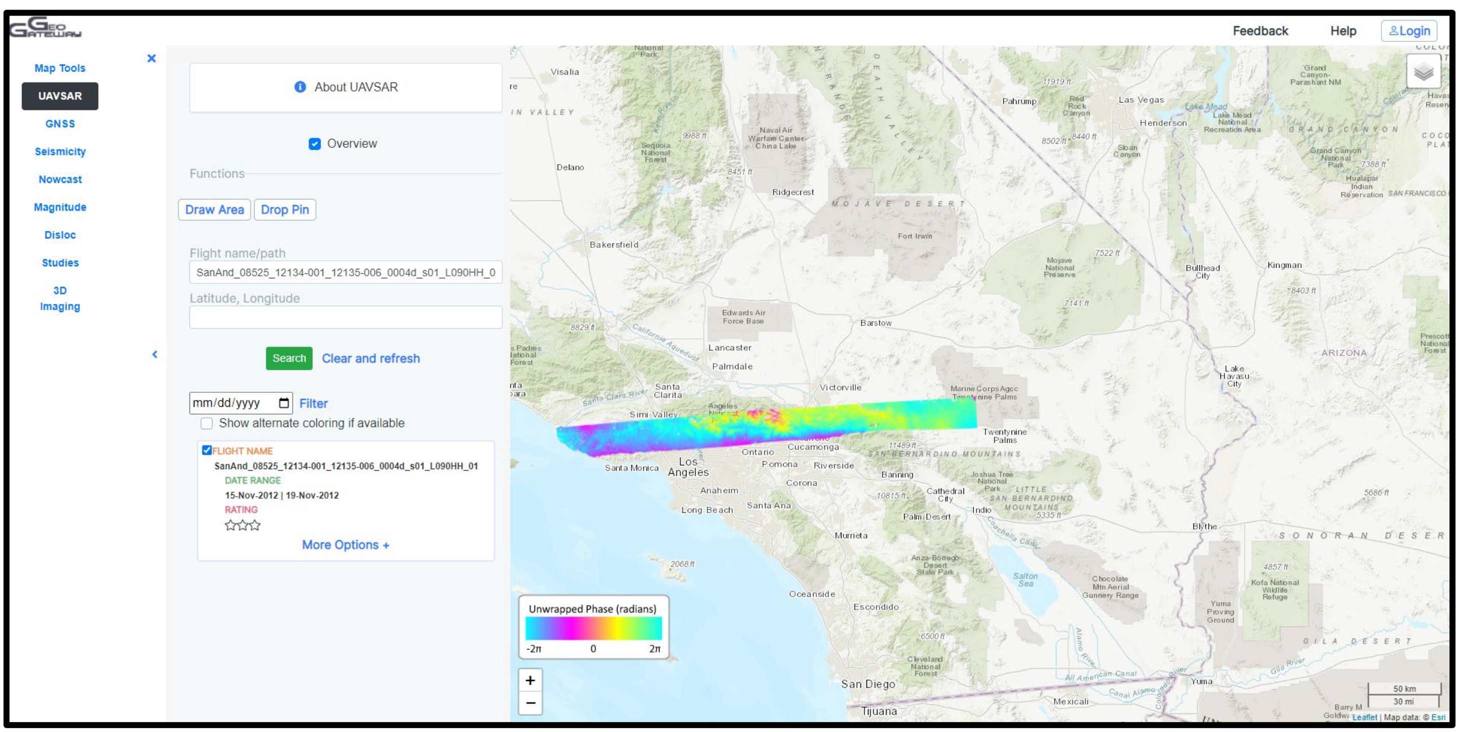

Figure 4: Demonstrates option 1 (inputting flight name/path)

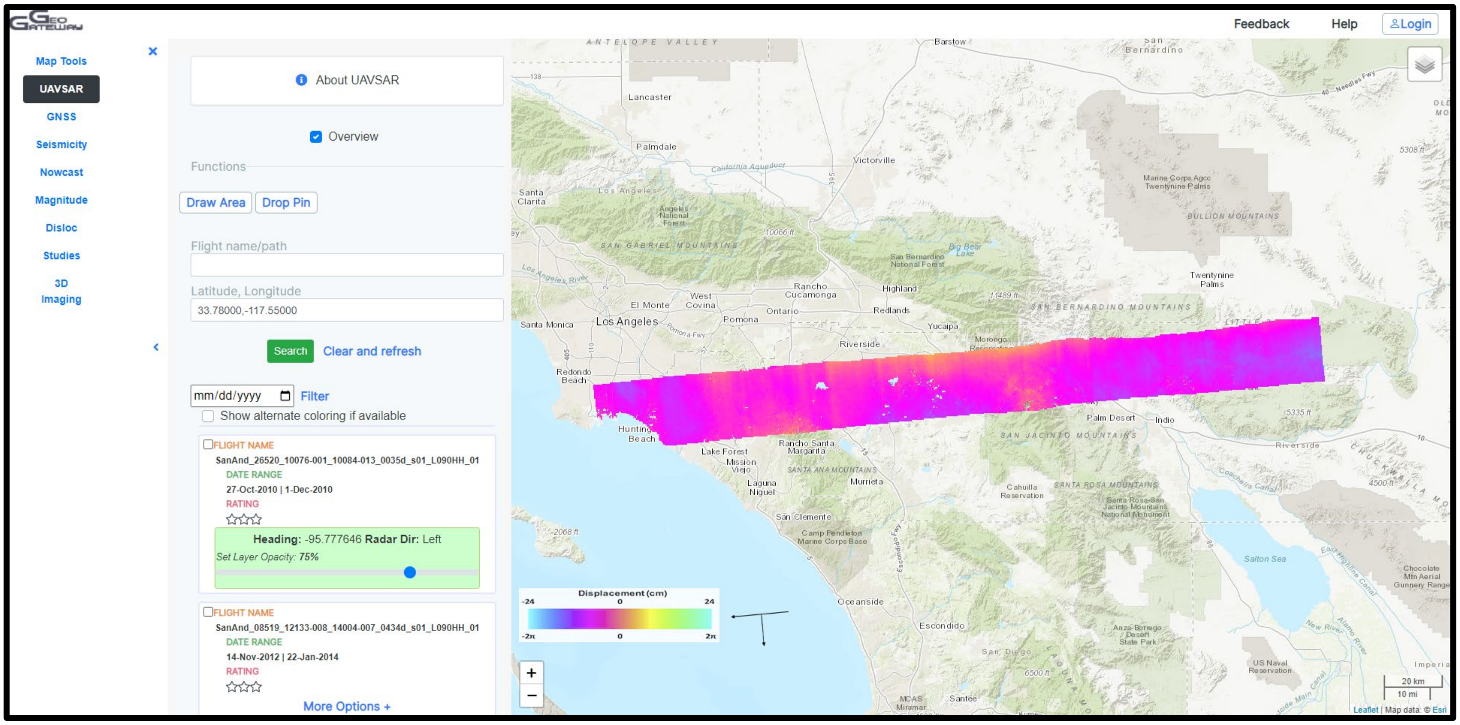

Figure 5: Demonstrates option 2 (inputting a latitude and longitude)

As shown in *figure 5* the option is given to filter by date by inputting (mm/dd/yyy), narrowing the selection.

To further look into the surface fracturing, click on "Show Alternate Coloring" below the "Filter by Date" option. Notice the units of displacement change to "cm." *Note to set the swath opacity, move the blue dot to the left (less visibility) or right (more visibility).

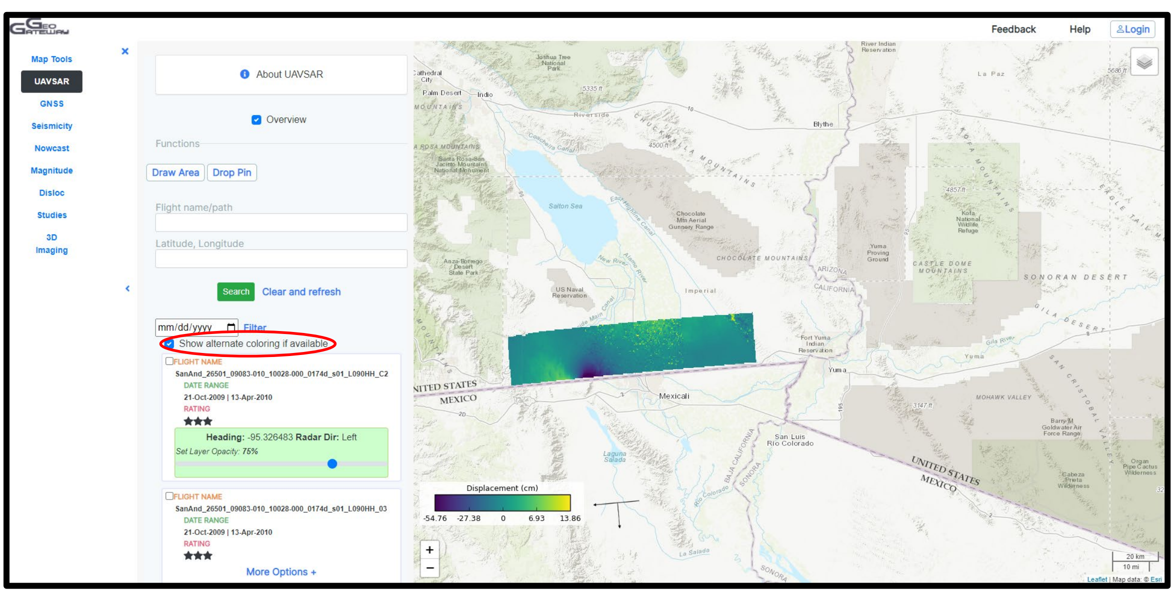

Figure 6: Demonstrates the change from the original unwrapped phase from figure 5, to displacement.

To look closer into the UAVSAR swaths,

1. Search for a flight path.
2. Select the flight path by clicking on it (flight path selection should be a darker color from the unselected paths).
3. Click on the UAVSAR flight path that is shown on the map, allowing the Line-of-Sight (LOS) tool (green dots) and elevation data (blue line) to appear.

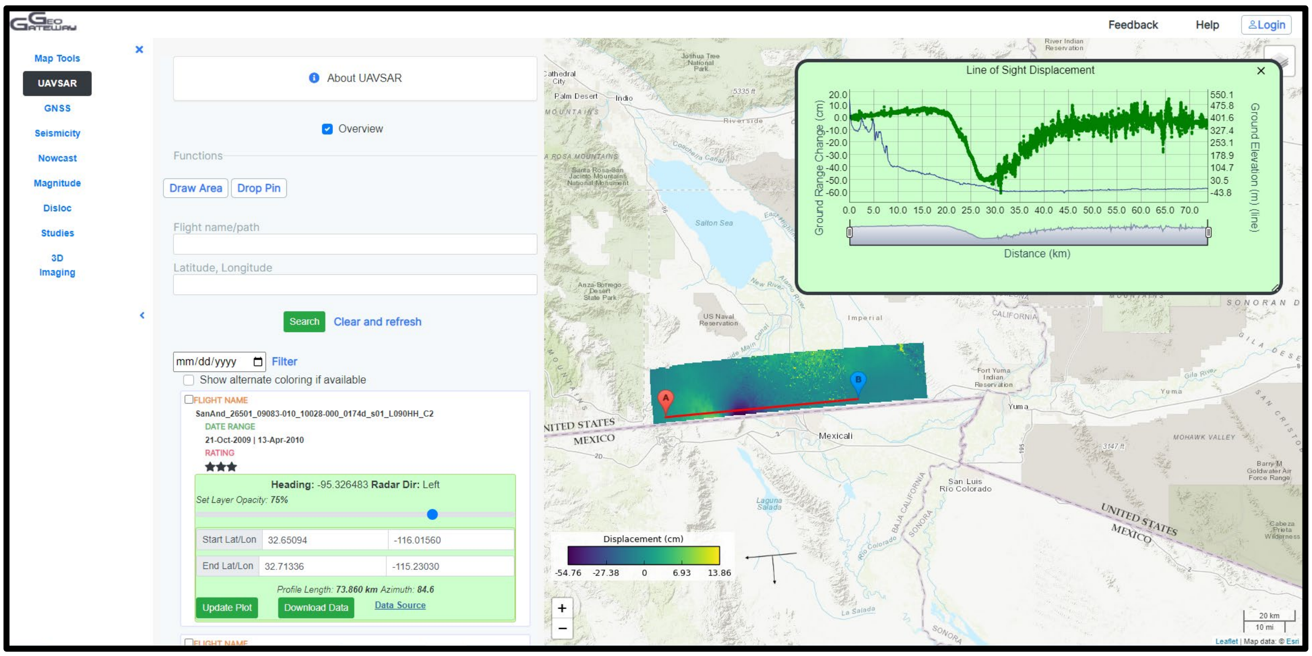

Figure 7: Line-of-Sight tool

Place the two markers on any location along the UAVSAR swath, to look at different ground range change.

The LOS tool allows users to study ground range change (cm), along a distance (km).

Positive values correspond to relative motion toward the radar.

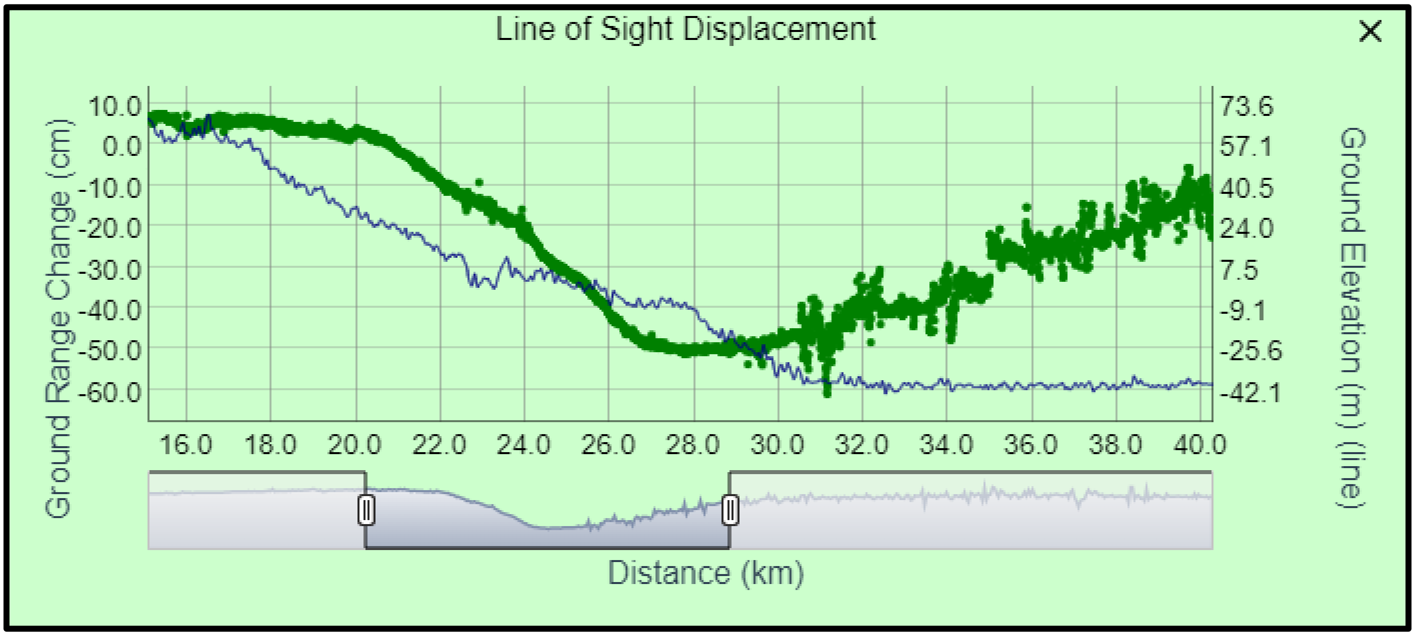

Figure 8: Line-of-Sight tool set to specific distance

Users are able to choose a distance of focus by moving ▯ as shown in *figure 8*.

GNSS

Global Navigation Satellite System (GNSS) is any satellite constellation which provides positioning, navigation, and timing (PNT) services on a global or regional basis (*Other Global Navigation Satellite Systems (GNSS)*, 2020). One of the systems GNSS includes is the United States-owned Global Positioning System (GPS).

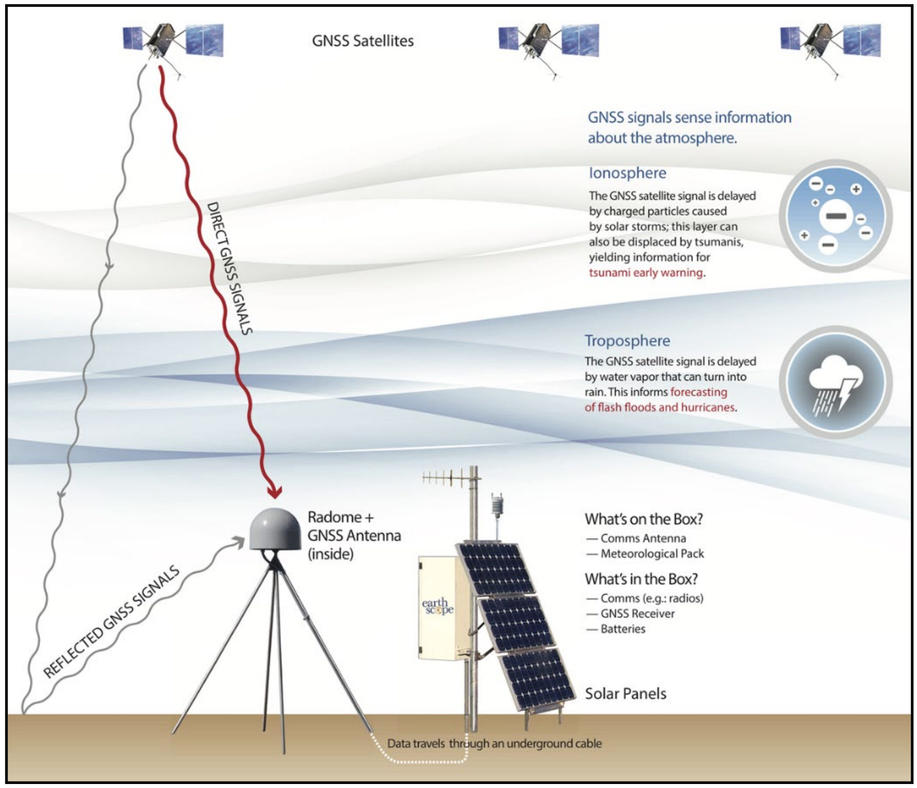

Figure 1: Network of the Americas (NOTA) GNSS station portraying the primary components of the platform. (Figure adapted from (UNAVCO, 2020))

GNSS operates via satellites sending information on two radio-frequency carriers to the receivers on earth as shown on *figure 1*. The GNSS receivers have both an antenna and processing unit. The antenna receives the satellite signals, and the receiver processes the information and turns it into measurements.

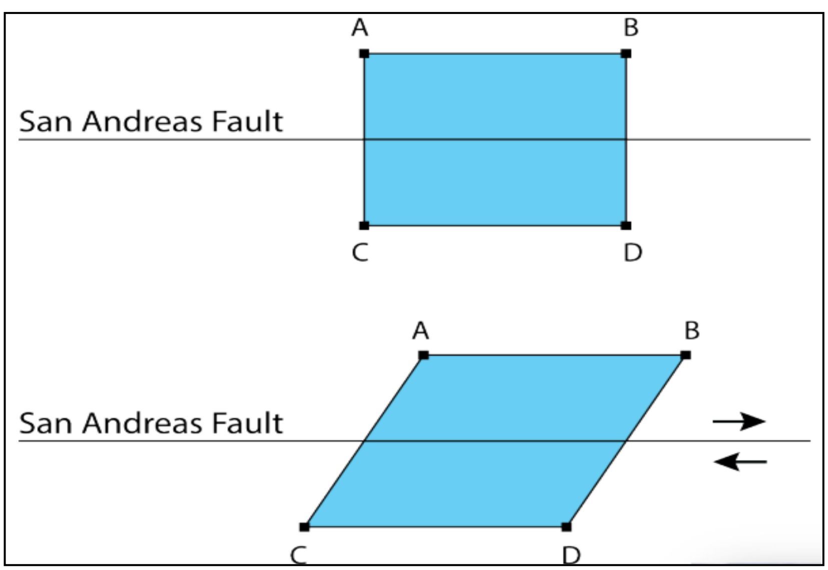

Figure 2: Demonstrates how GNSS data detects fault movement along the San Andreas Fault. (Figure adapted from (USGS, n.d.))

GeoGateway's GNSS tool can be used to measure plate motion and strain accumulation across faults. *Figure 2* demonstrates how fault motion is measured along a segment of the San Andreas Fault. The top of the figure (square shape) demonstrates the initial state of the fault at the date of observation, while the bottom of figure (parallelogram) shows how at a later date of observation, the fault has moved.

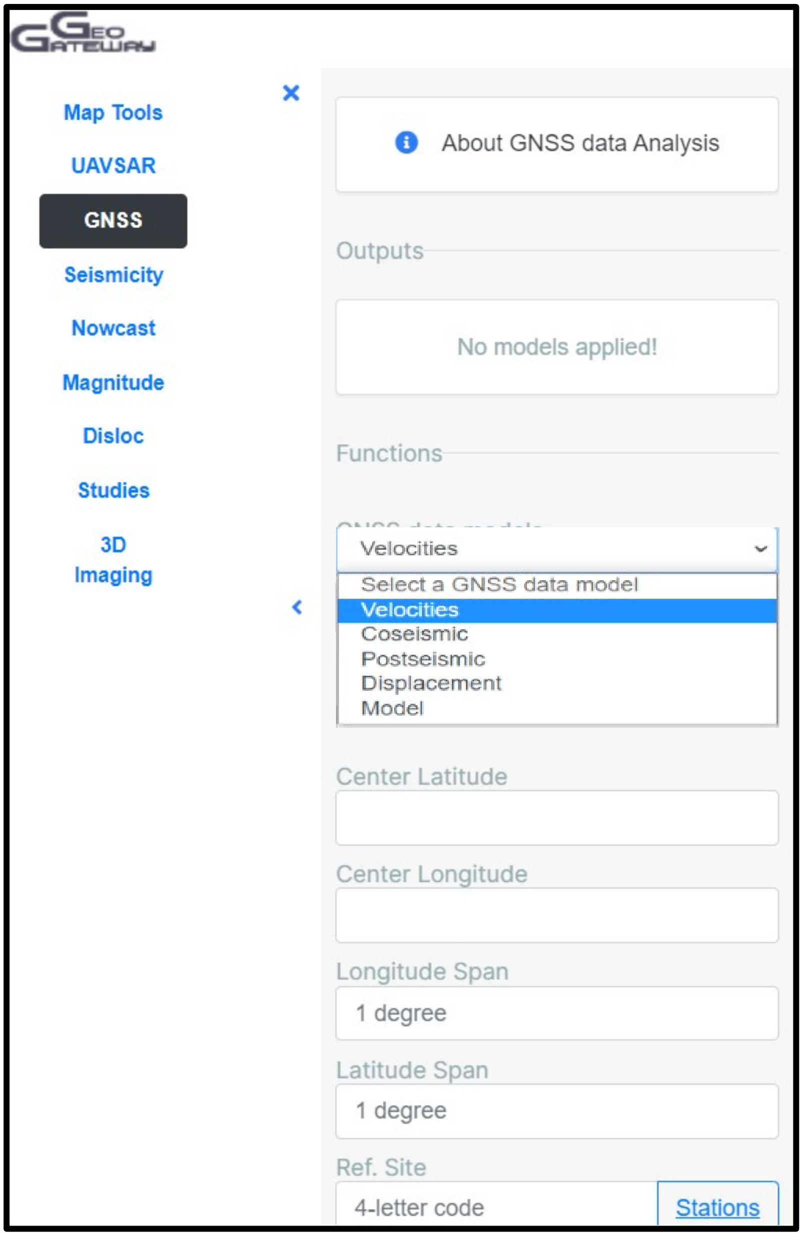

Figure 3: GeoGateway's GNSS tab, which includes five options of analysis; Velocities, Coseismic, Postseismic, Displacement, and Model.

GeoGateway offers five tools for analyzing GNSS data as shown in *figure 3*. Note the parameters in bold are required and the remaining parameters that are not in bold use default values set by GeoGateway which will be discussed within this section.

(option 1) Velocities
(option 2) Coseismic
(option 3) Postseismic
(option 4) Displacement
(option 5) Model

Parameters

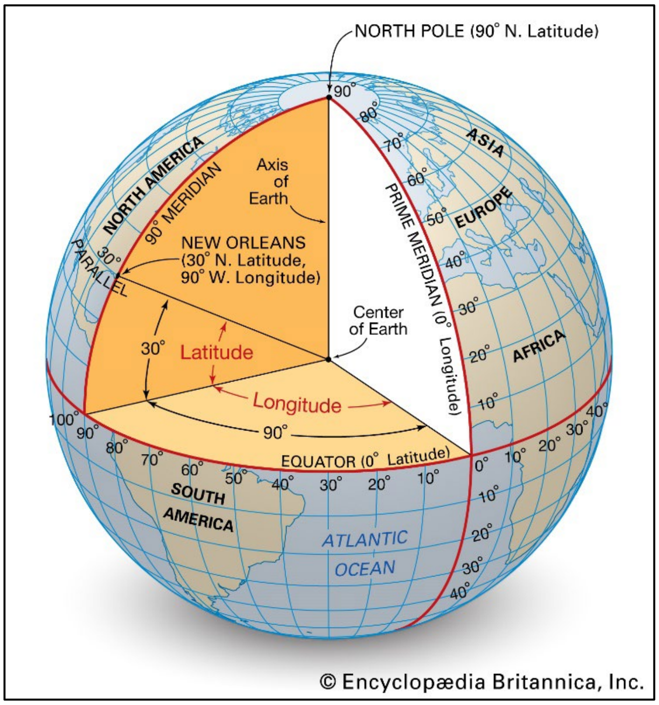

Figure 4: Overview of the geographic coordinate system (Figure adapted from (Britannica, n.d.))

Center Latitude (see *figure 4*) in decimal degrees
Center Longitude (see *figure 4*) in decimal degrees

*Positive latitude is above the equator (N), and negative latitude is below the equator (S). Positive longitude is east of the prime meridian, while negative longitude is west of the prime meridian.

Longitude Span and **Latitude Span** are measured in degrees, allowing the user to create a specified parameter.

Ref. Site is the GNSS station site that the velocity vector data will be referenced to. A map with the sites can be located through the website listed below, or users may access the list of sites by clicking on "**Stations"** in the Ref. Site section of the GNSS tab. Once a location is chosen, type the 4-letter code in the box.

https://sideshow.jpl.nasa.gov/post/series.html

Scale allows the user to control the velocity vector length scaling.
Recommend setting to **320** mm/yr/deg.

Output Prefix allows users to name the dataset output.

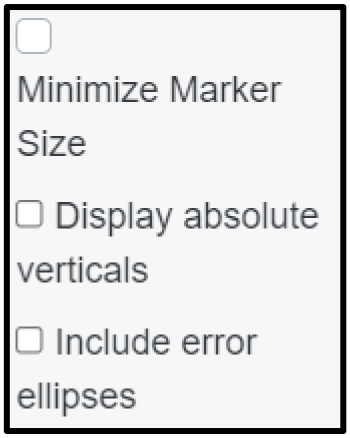

"Minimize marker size"  allows users to make GNSS site markers smaller as shown in the image below.

"**Display absolute verticals**"

Error bars are graphical tools used to illustrate the pair-wise correlation that exists between computed values (Error Ellipses). By checking the box **"Include error ellipses,"** a black ellipse at the tip of the velocity vector, representing error is displayed, as shown in the image below.

Once data is inputted, click on “Run”. There is an option to download the velocity text table and the horizontal and vertical KML files as shown in the image on the right.

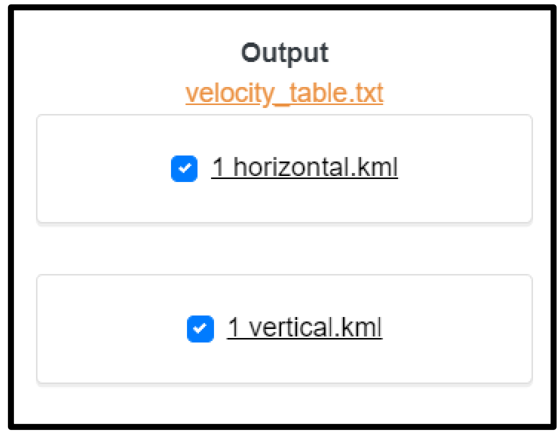

By selecting the “Velocities” option, the velocities of different GNSS stations are seen relative to the reference frame.

As shown in *figure 5* below “CCCC” is set as the reference point.

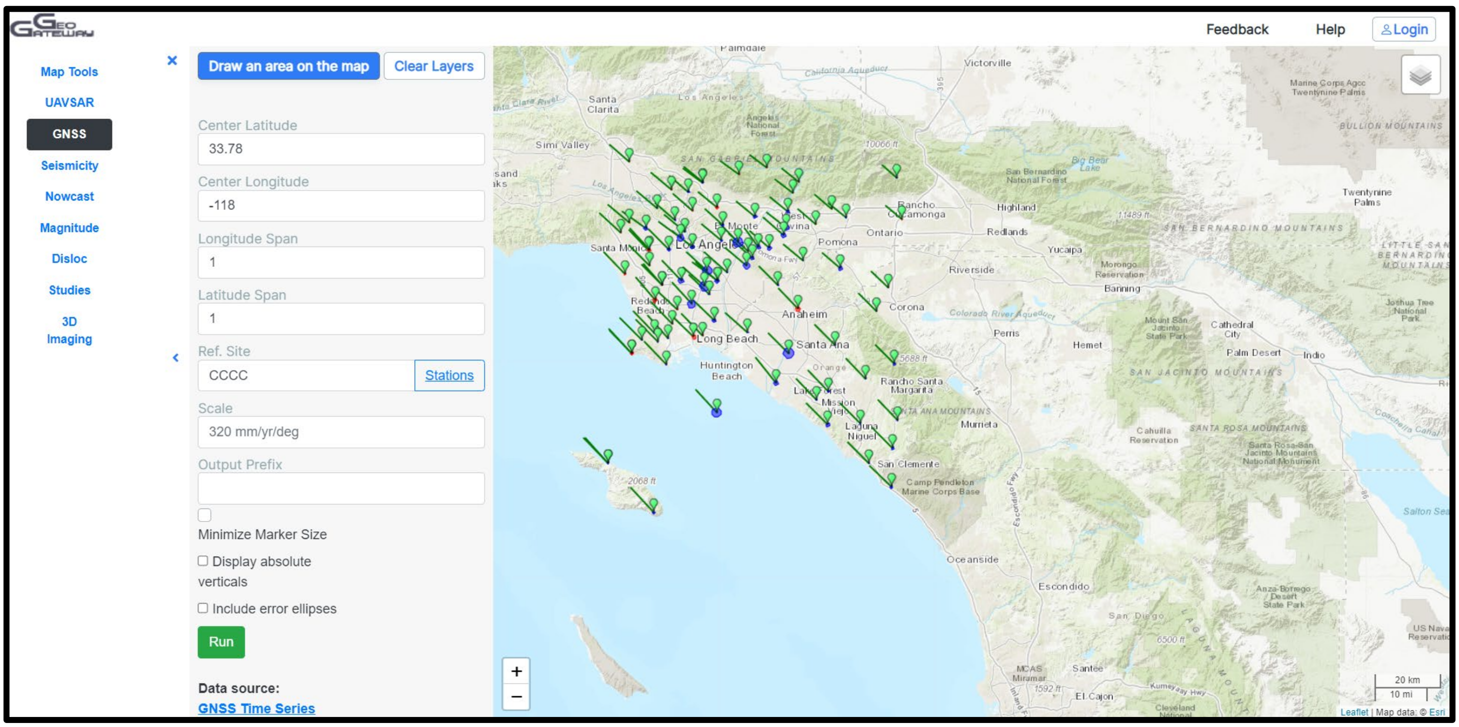

Figure 5: Velocities Analysis

Each vector shows the velocity of a single GNSS station as the Earth moves.

The tail of the vector is pinned at the GNSS station, and the length of the vector shows how fast the GNSS station is moving. The other end of the line, away from the marker, is the direction the GNSS station is moving.
Vertical displacements are shown by red (uplift) or blue (subsidence) circles. The larger the circle, the more displacement.

By clicking on a GNSS station, three time series graphs appear.

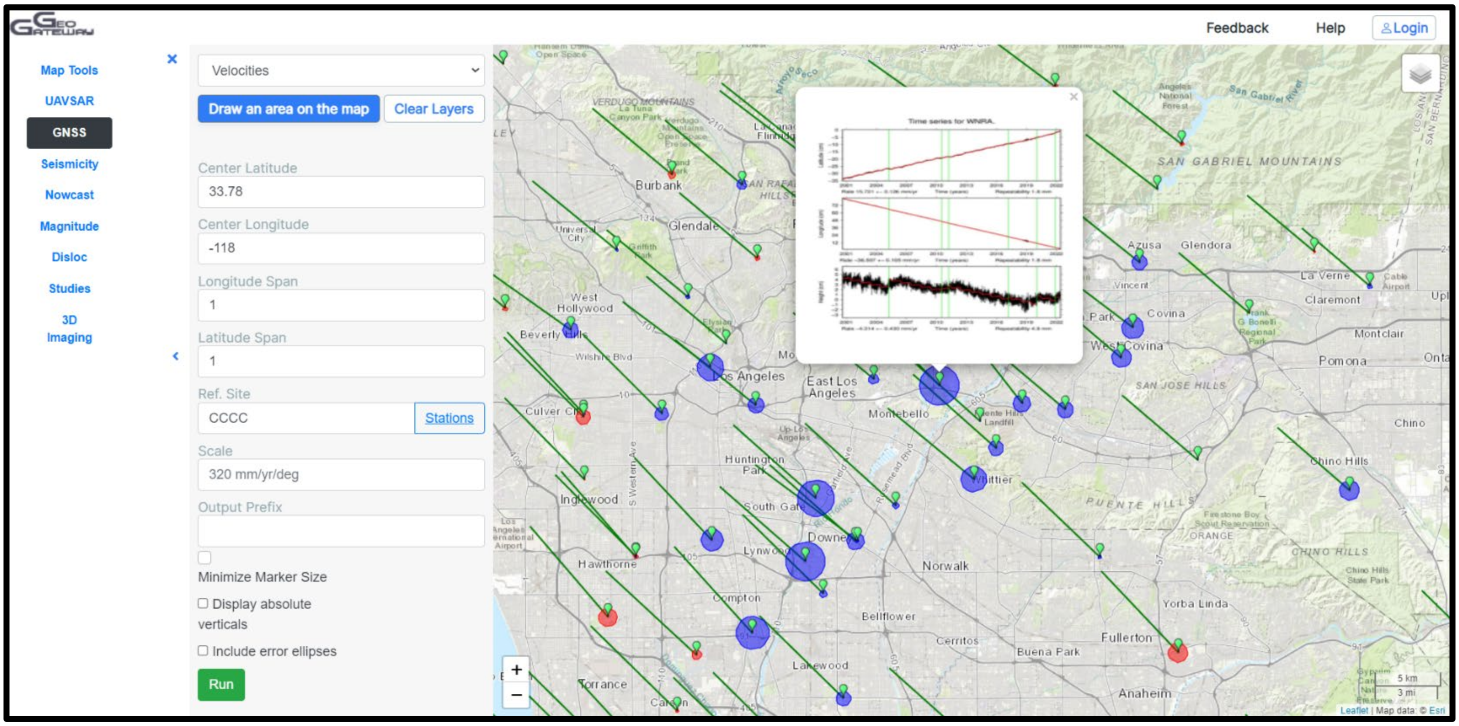

Figure 6: Time Series for WNRA station

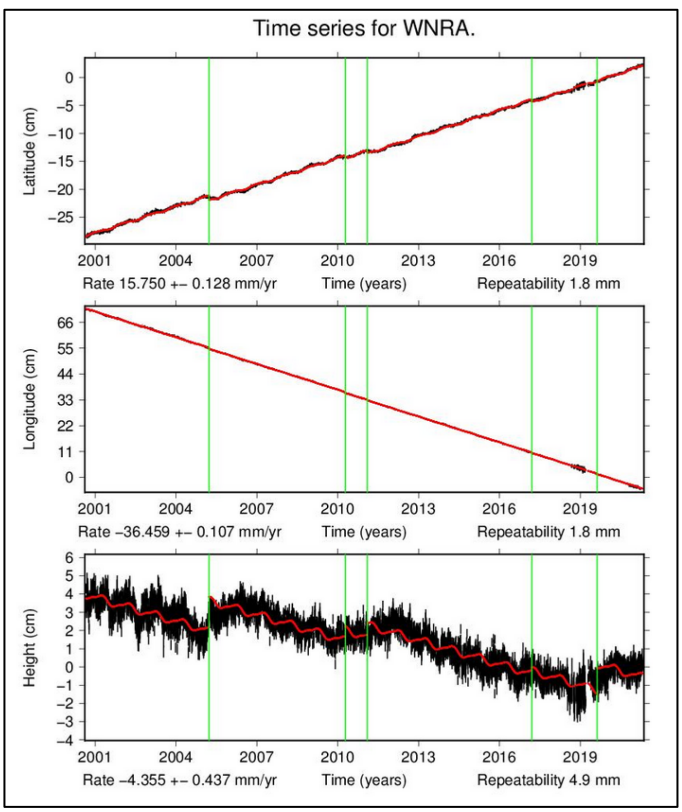

Figure 7: Time series tables, including latitude, longitude, and height

The time series shows how far the station has moved. The top graph shows latitude (cm) versus time (years). The black dots are the data points and the red line is the best fit line to the entire dataset. In this example, we see as time progresses the station moves closer to the North. For the longitude versus time graph (middle graph) we see that the GNSS station is moving to the West. The bottom graph shows the vertical height versus time which is decreasing. The green lines that intersect vertically on the graph are locations where there are jumps in the data.

Coseismic and postseismic data can be selected by specifying a time period during or after an earthquake which a user wants to focus on.

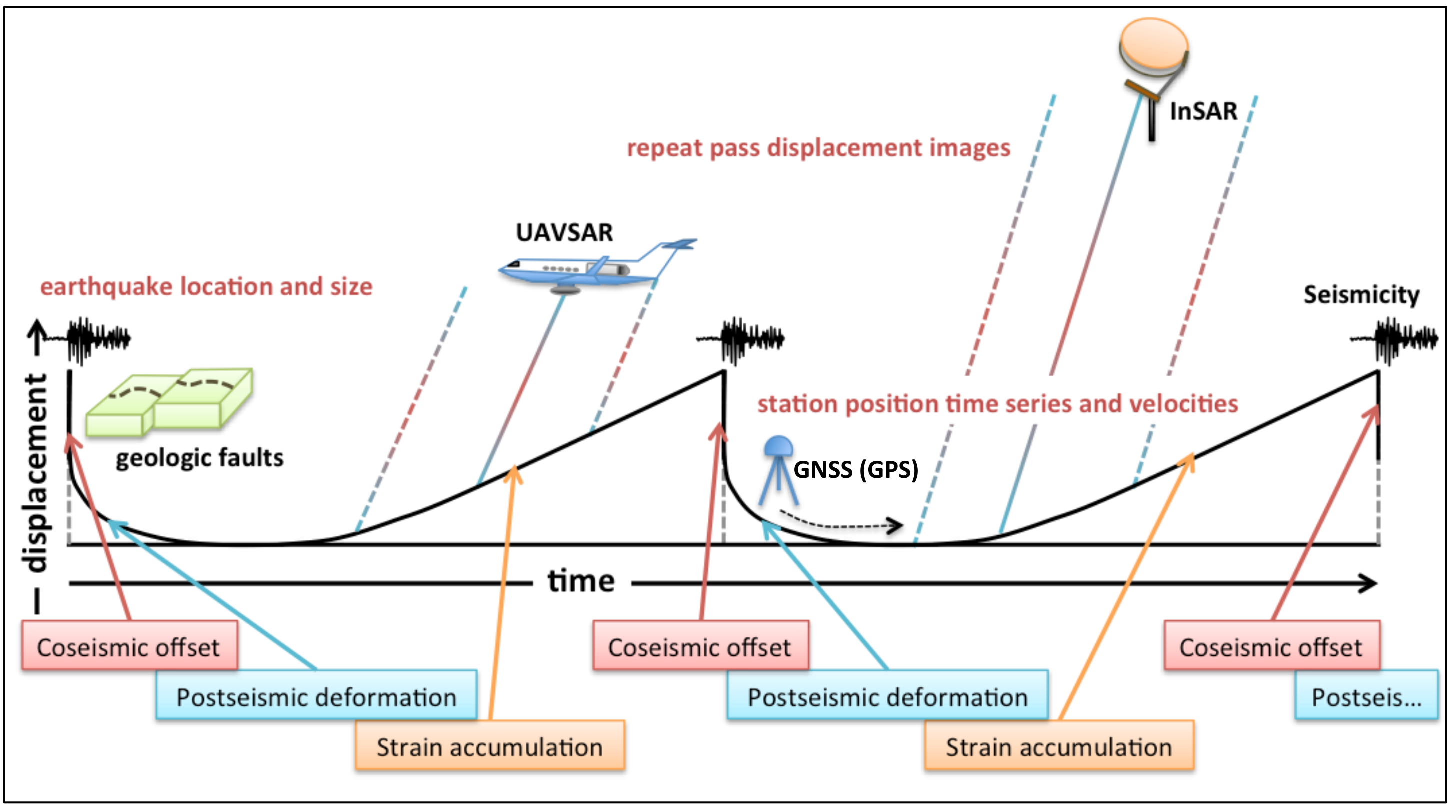

Figure 8: Crustal deformation is spatially and temporally non-uniform as strain accumulates over prolonged time scales, where its later rapidly released as earthquakes, and readjusts post-seismically. Numerous types of data from different sections of the earthquake cycle (as shown in the figure above) are required for analysis.

Figure 8 illustrates the earthquake cycle, and typical rates of deformation in the coseismic and postseismic periods.

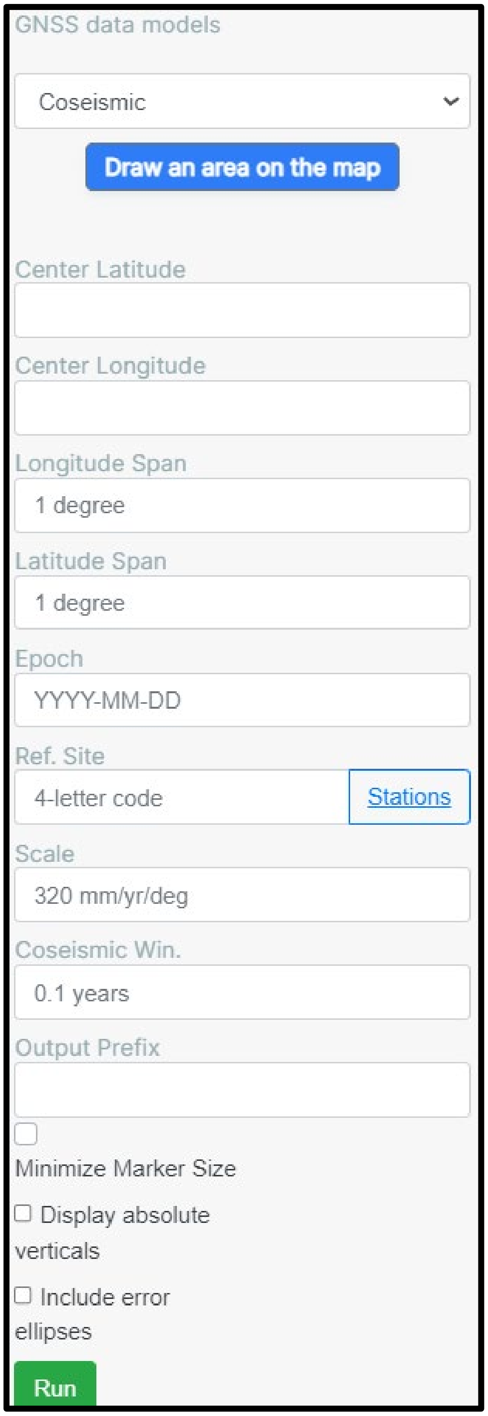

Figure 9: Coseismic offset refers to the time during an earthquake until a rupture ends.

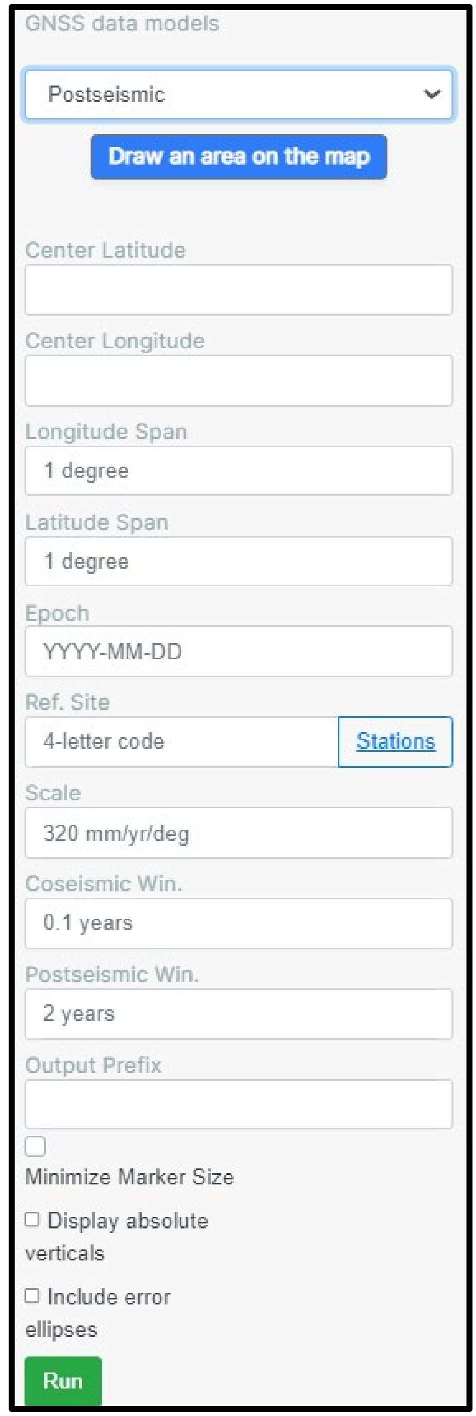

Figure 10: Postseismic deformation refers to the time after a large earthquake when deformation occurs.

To generate coseismic and postseismic displacements, the user must consider "Epoch" and "Coseismic Window" and "Postseismic Window." The Epoch is the time of the event and the window is any time period of choice.

The displacement tool avoids use of any fit parameters and instead uses daily time series data to directly compute displacements between any two times which have measurements (Heflin et al., 2020).

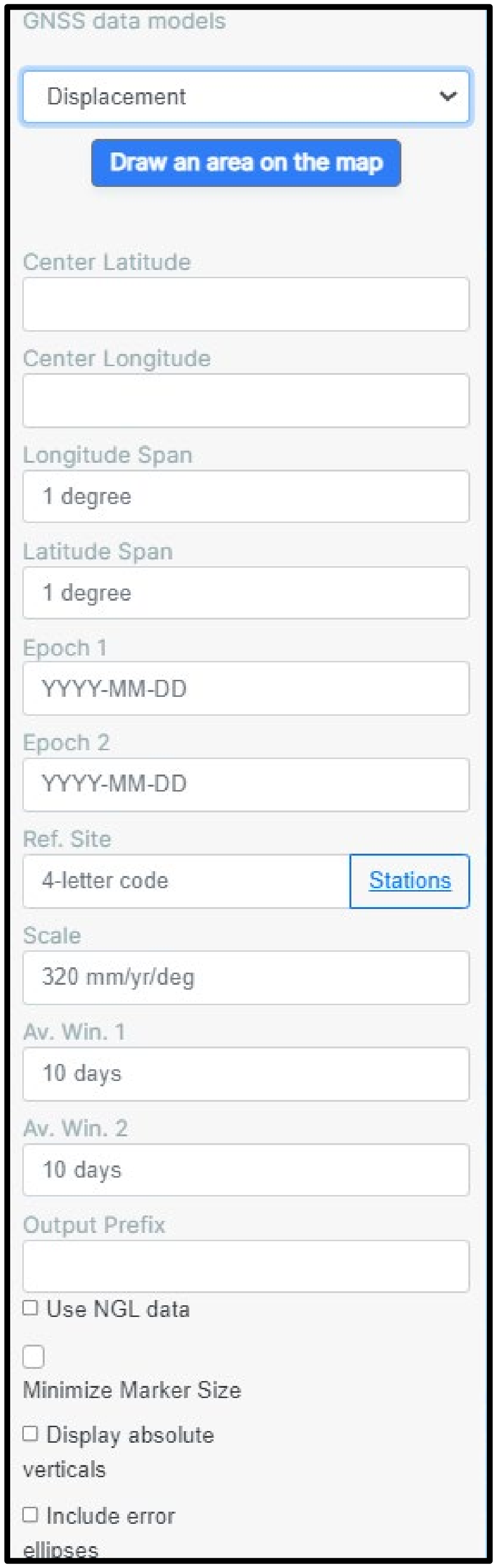

Figure 11: Displacement Analysis

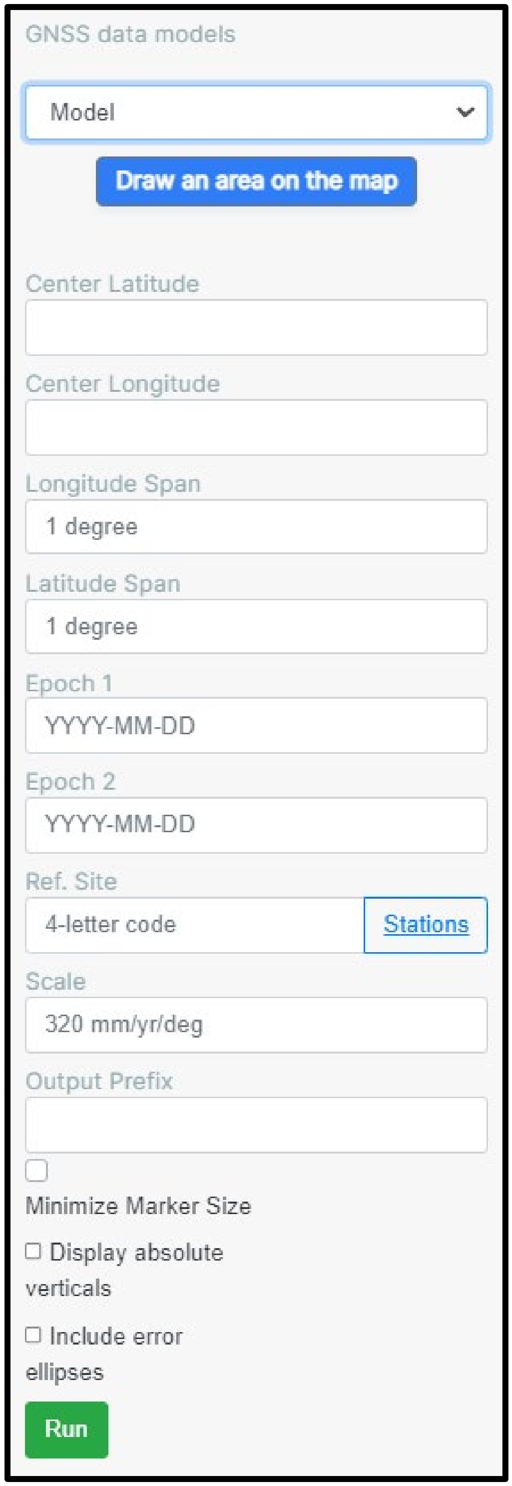

Figure 12: Model Analysis

The model tool uses all fit parameters to compute a displacement between two user specified times (Heflin et al., 2020).

Seismicity

The seismicity tab allows users to display earthquakes in a region over a specified period. *Figure 1* displays GeoGateway's Seismicity tab. The tab is split into two sections, "Recent Earthquakes from USGS" and "Search Earthquake Catalog."

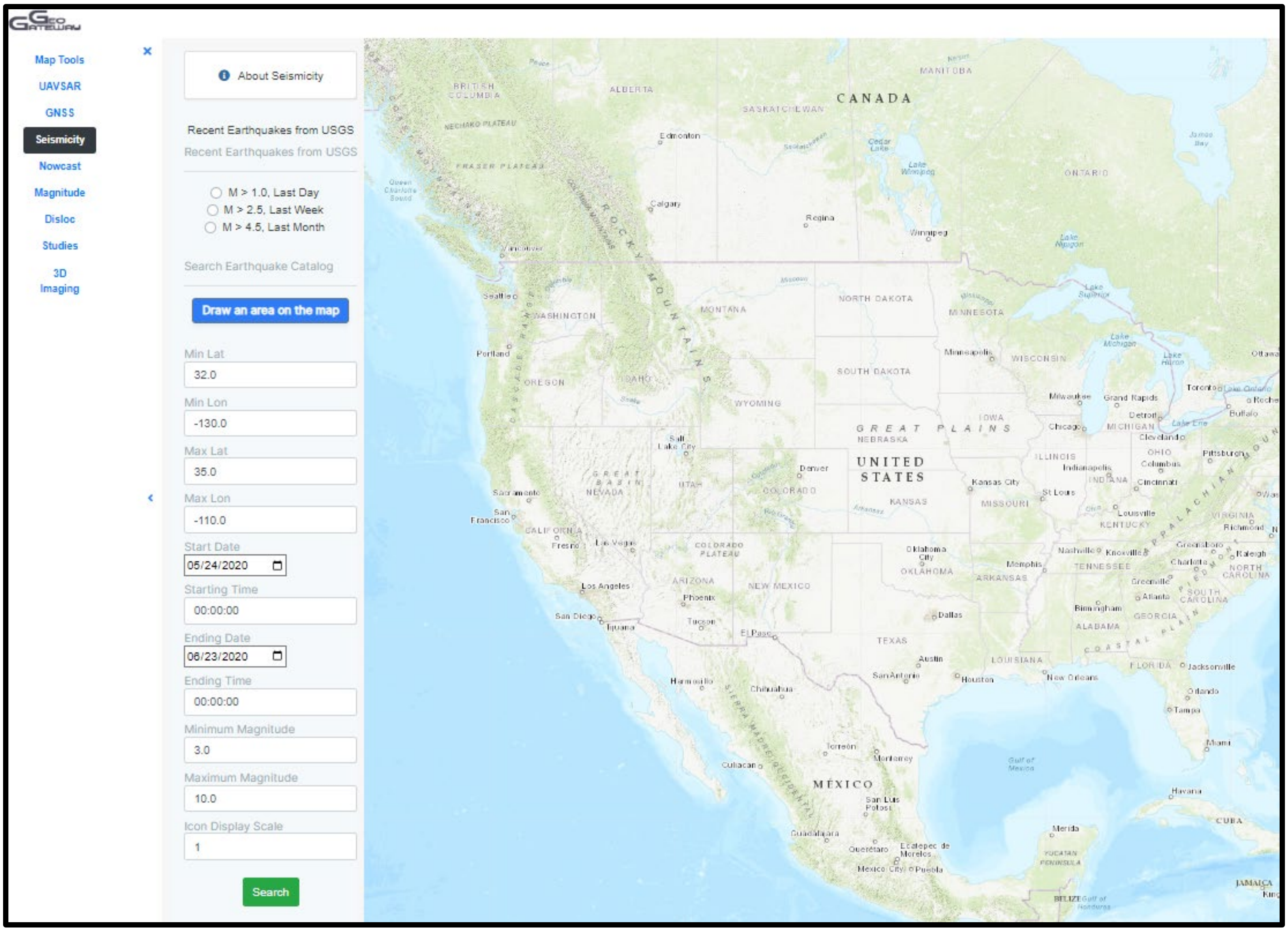

Figure 1: GeoGateway's Seismicity tab

The tab allows users to view recent earthquakes from USGS data. The USGS data can also be found on the USGS website earthquake.usgs.gov/earthquakes/map/. As shown in *figure 2*, the displayed earthquake events are color coded with the hotter colors representing recent events and the cooler colors representing less recent events.

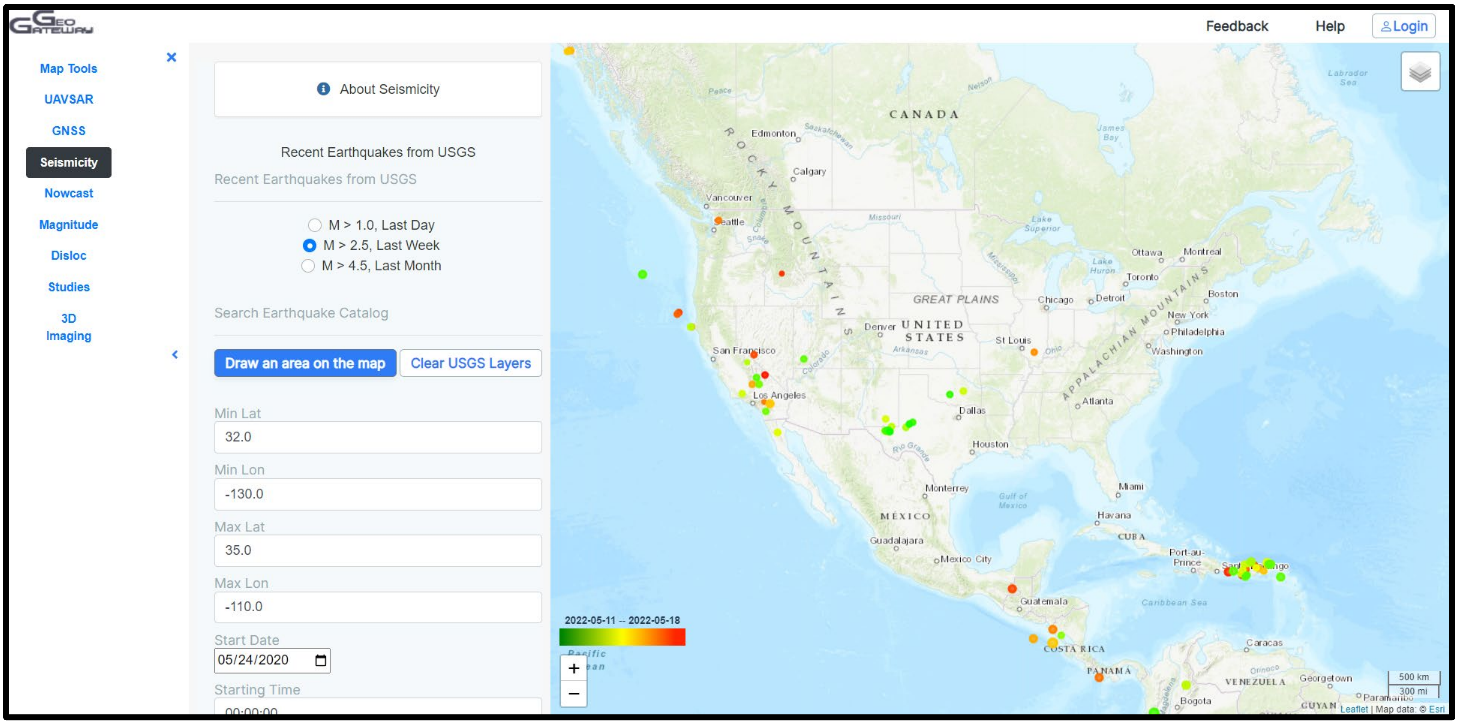

Figure 2: GeoGateway's Seismicity tab - displaying seismic events greater than magnitude 2.5 in the last week.

Filters, such as **M > 1.0, Last Day**, **M > 2.5, Last week**, and **M > 4.5, Last Month** can be selected as shown in *figure 2*. As shown below, additional filters may be applied to generate recent earthquakes.

To search for a particular earthquake event, input specific parameters pertaining to the event in the **Search Earthquake Catalog** section.

Box 1-4 require users to input the latitudes and longitudes of the specified region. Users have the option to use the "Draw an area on map" feature to generate earthquake events onto the map based on the region drawn by the user.

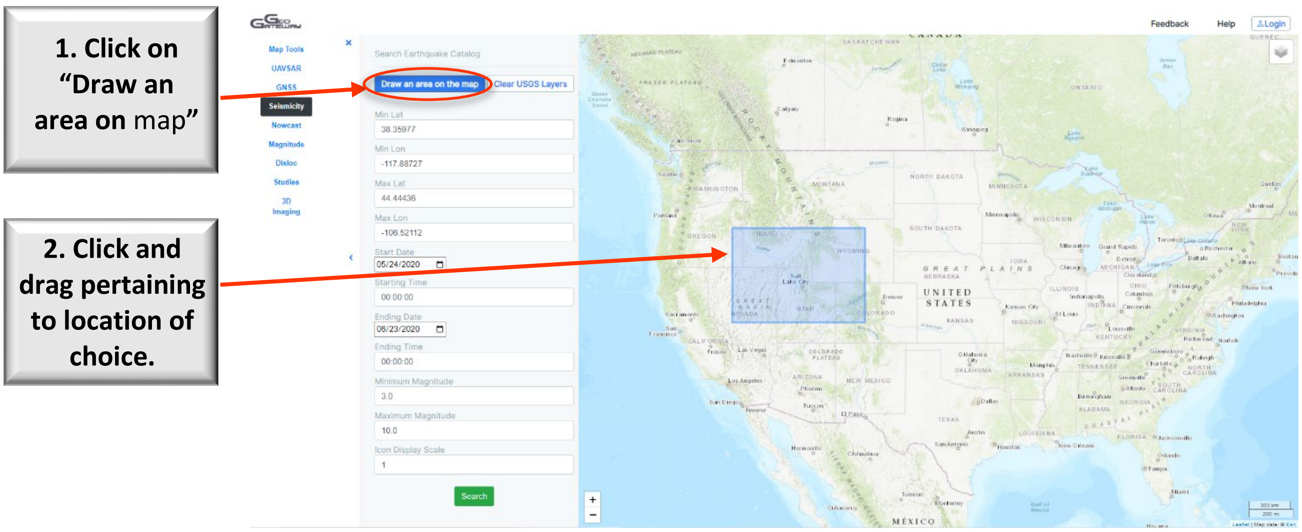

Figure 3: Draw an area on map option

Box 5-8 require data regarding the range of date and time of interest.
Box 9-10 require the range of chosen magnitude.
Box 11 requires the user to scale the size of the icon of the earthquake event, by inputting a number (larger number = larger icon).

By clicking on **Search Catalog** earthquake events based on the given parameters inputted by the user are shown on the map.

To clear the inputted USGS data, click on **Clear USGS Layers** right below to **Draw an area on map** option.

Moreover, users are given the option to download "USGS KML" and "GeoJSON."

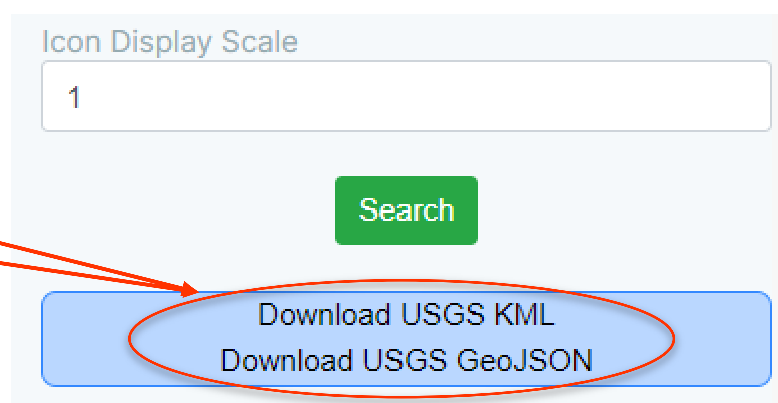

Figure 4: Download USGS KML and GeoJSON.

Magnitude

Magnitude is the physical size of an earthquake. In *figure 1*, notice the magnitude scale in correspondence to the earthquake's energy equivalence.

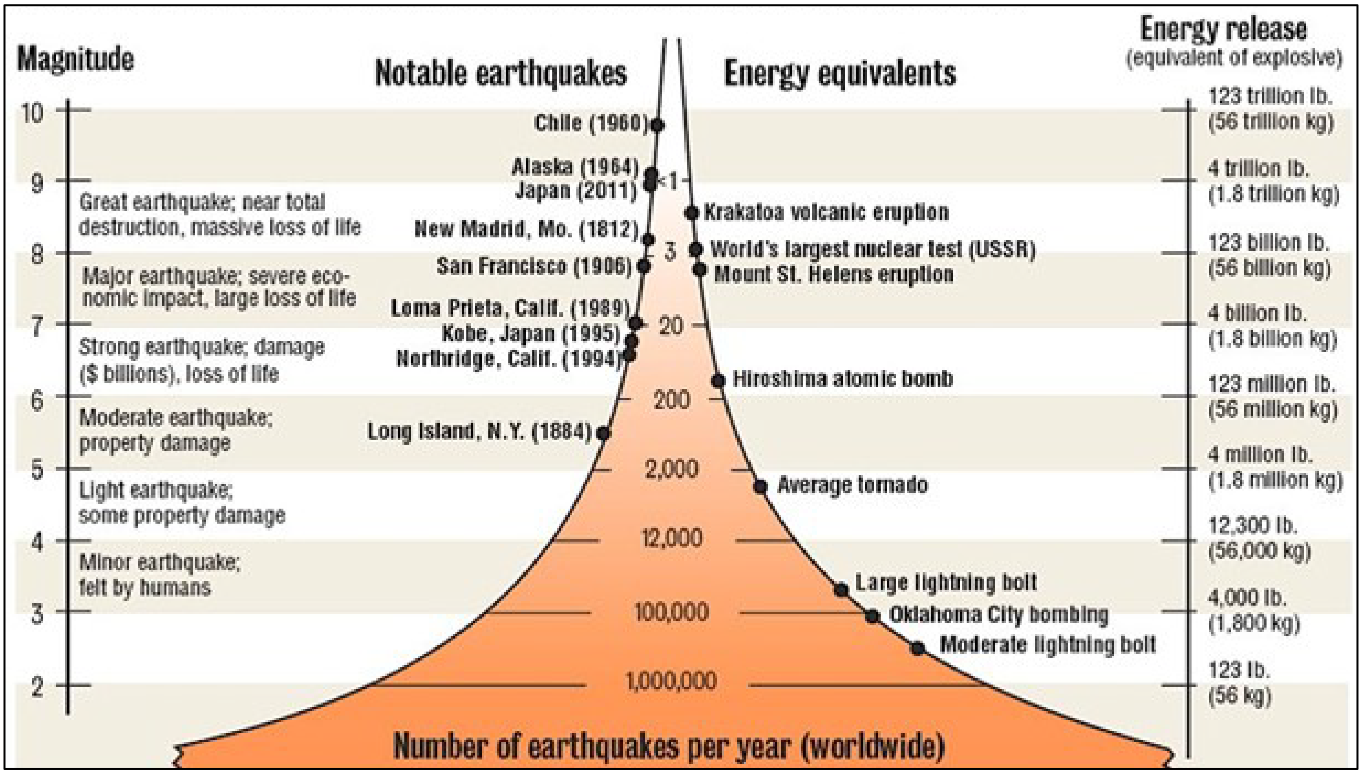

Figure 1: Seismic wave energy in earthquakes and energy equivalents. (Figure adapted from (Incorporated Research Institutes for Seismology, IRIS))

Both seismic moment and moment magnitude (**Mw**) can be calculated using GeoGateway's moment magnitude calculator. As shown in *figure 2*, **seismic moment** equates to the product of the shear modulus (μ), displacement (D), and rupture area (A), and **moment magnitude** equates to the product of two-thirds the log base of seismic moment, subtracted by 10.73.

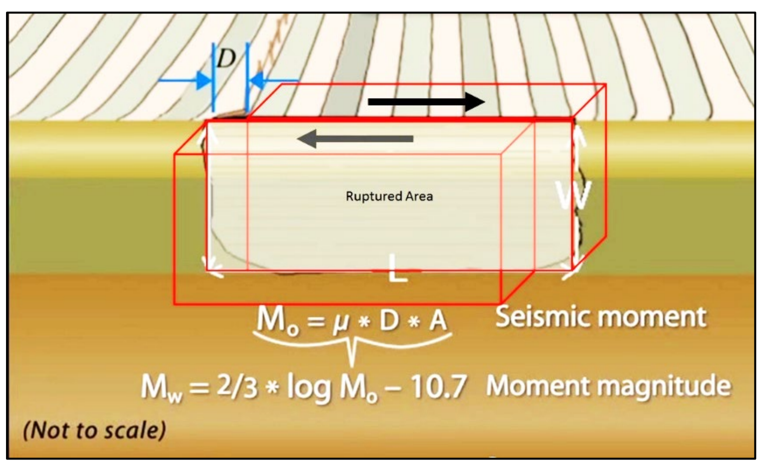

Figure 2: Represents the seismic moment and moment magnitude equations. (Figure adapted from (Vista Heights Middle School))

The shear modulus (μ) is

3.2×10^{11} dynes/cm^2 in the crust
7.5×10^{11} dynes/cm^2 in the mantle

The area (km^2) as shown in *figure 2* can be found by using the length (L) and width (W), of the rupture. The slip (meters) is the average displacement (D) of rupture.

Step 1: To begin calculations, click on the "Magnitude" tab

Step 2: Once the tab is open, input the fault length that ruptured in kilometers

Step 3: Input the fault width that ruptured, in units of kilometers

Step 4: Input the distance the fault moved (slip), in units of meters

Step 5: Input the shear modulus in units of $\frac{10^{11} dyne}{cm^2}$

Step 6: Click on Calculate

GeoGateway has set a default moment magnitude similar to the 2014 Napa, CA earthquake. The results indicate a seismic moment of 1.7×10^{25} dyne*cm and a moment magnitude of 6.1.

Step 1: navigate to the Magnitude tab
Step 2: input the length
Step 3: input the width
Step 4: input the slip
Step 5: input the shear modulus

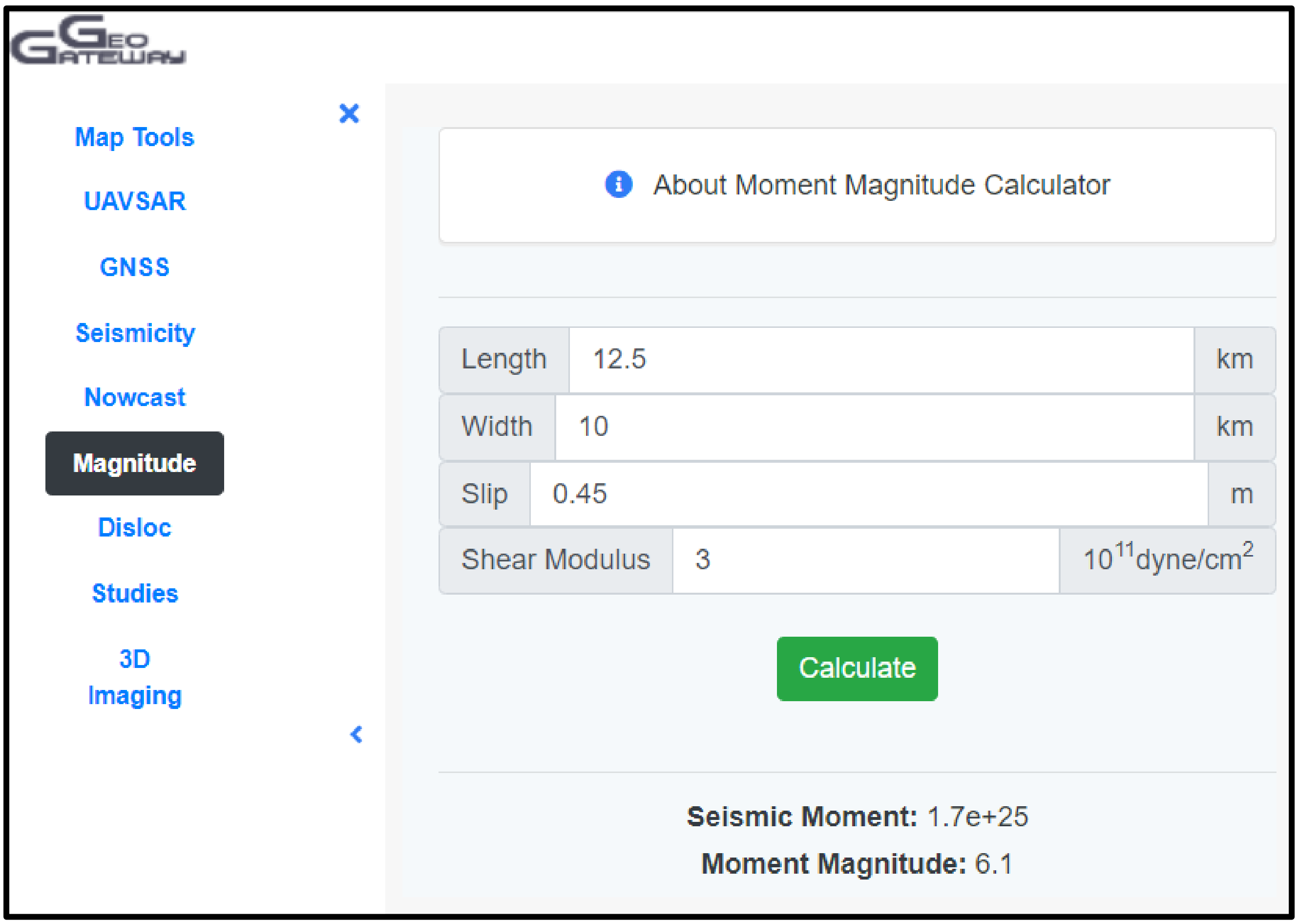

Figure 3: Calculating seismic moment and moment magnitude of the 2014 Napa, CA earthquake.

Disloc

Elastic dislocation models are commonly used to analyze inversion on faults following an earthquake (Chen et al., 2020). In 1985, Yoshimitsu Okada (Ph.D.) proposed a formula which calculated displacement in an isotropic, uniform elastic half space. The formula can calculate coseismic deformation caused by any fault within the elastic half space (Okada, 1985). Okada's dislocation theory, which is the most commonly used dislocation theory, is often used with InSAR. InSAR monitors the surface coseismic deformation field, and subsequently, Okada's theory is used to conduct fault slip inversion, calculating the coseismic strain stress field (Chen et al., 2020). Elastic dislocation models generated by Disloc can be used to geodetically measure deformation of an elastic medium due to slip from active faults (Avouac, n.d.).

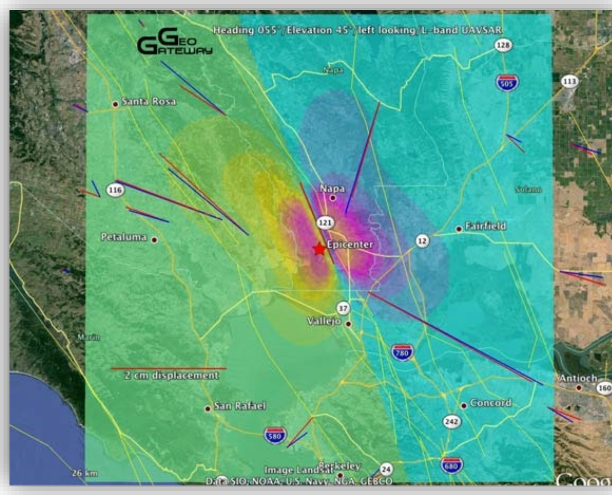

Figure 1: Example of Okada's dislocation in an elastic half space (figure adapted from NASA's GeoGateway team).

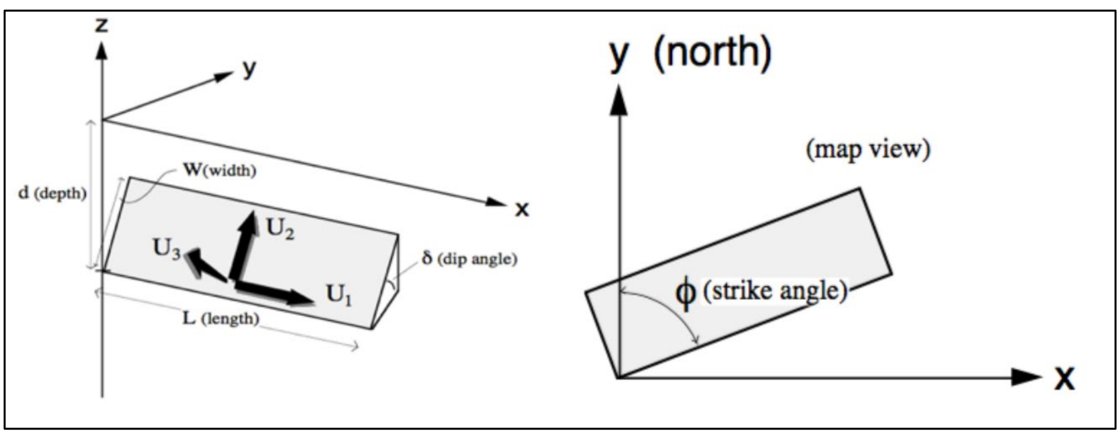

Figure 2: Elastic Dislocation Fault Parameters (figure adapted from Harvey Mudd College)

In *figure 2*, the ***location*** of the fault is defined as the surface projection of the lower-left corner of the fault plane. The ***depth*** is represented as the z-coordinate of the fault's bottom edge. The depth is the absolute value of the z-coordinate. The ***dip*** angle is measured from horizontal (Harvey Mudd College, n.d.).

The ***strike*** angle is the orientation (measured clockwise from north) of the surface projection of the fault's horizontal edges. The ***length*** and ***width*** are the dimensions of the rectangular fault (Harvey Mudd College, n.d.).

U_1 is the strike slip component of fault slip (strike-slip dislocation U_1 greater than 0 identifies a right lateral motion).
U_2 is the dip slip component of fault slip (dip-slip dislocation U_2 greater than 0 identifies a reverse motion).
U_3 is the tensile component of fault slip (tensile dislocation U_3 greater than 0 identifies a tensile opening).

To run Disloc, visit the Disloc tab on GeoGateway and follow the following steps.

Step 1: Create an account on GeoGateway by visiting https://geo-gateway.org/auth/create-account

Step 2: Log into GeoGateway by clicking on the Login button on the right corner found on GeoGateway's Map Tools' page.

Step 3: On the upper right corner on GeoGateway's homepage, click on "GeoGateway Develop," and then click on "Workspace."

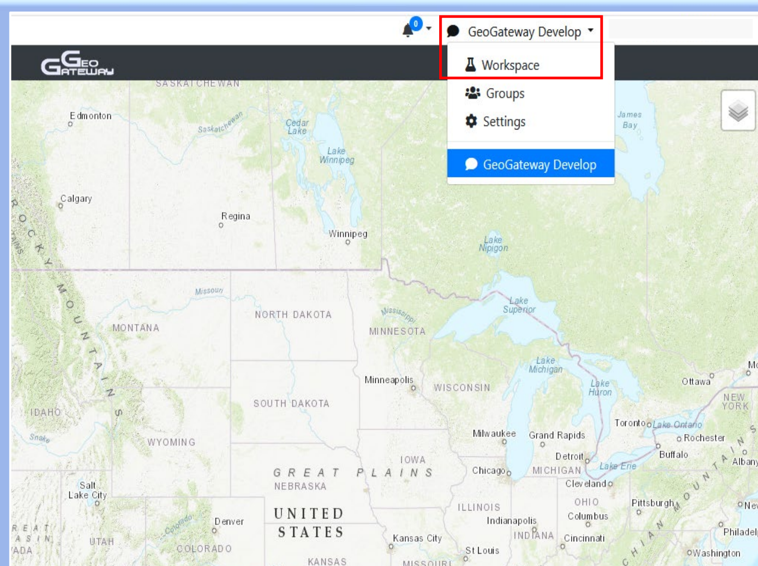

Step 4: Click on the “Disloc” application as shown within the red box.

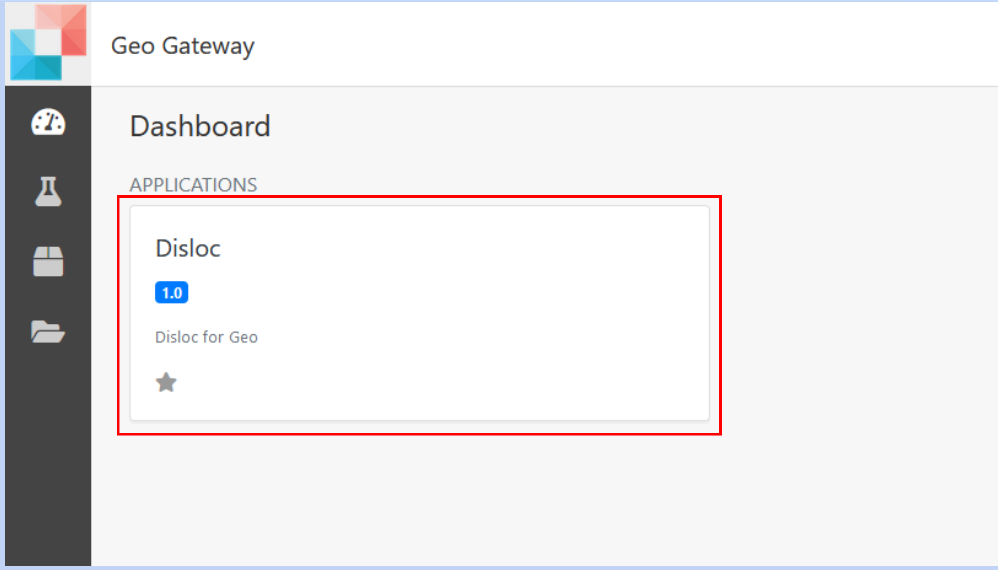

Step 5: Users must upload their Disloc files into the area shown in the red box. Users have the option to change the experiment name and add a description by clicking on “Add a description.” Users may also change the “elevation,” “azimuth,” and “radar frequency,” of their choice as shown in the image to the right. Lastly, click on the green button, “Save and Launch.” Note the data might take a couple of minutes to load.

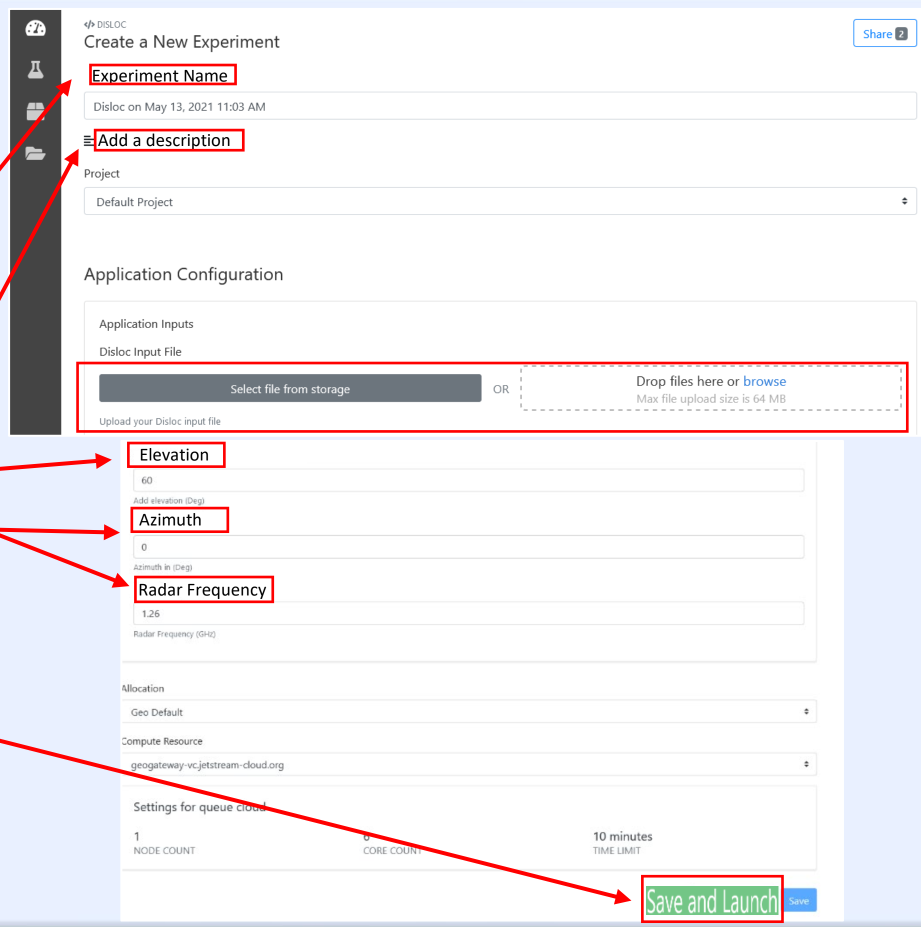

To find the output files, click on the Erlenmeyer flask found on the left side of the page. There the output file name will be displayed. To view the output files, click on the experiment of interest.

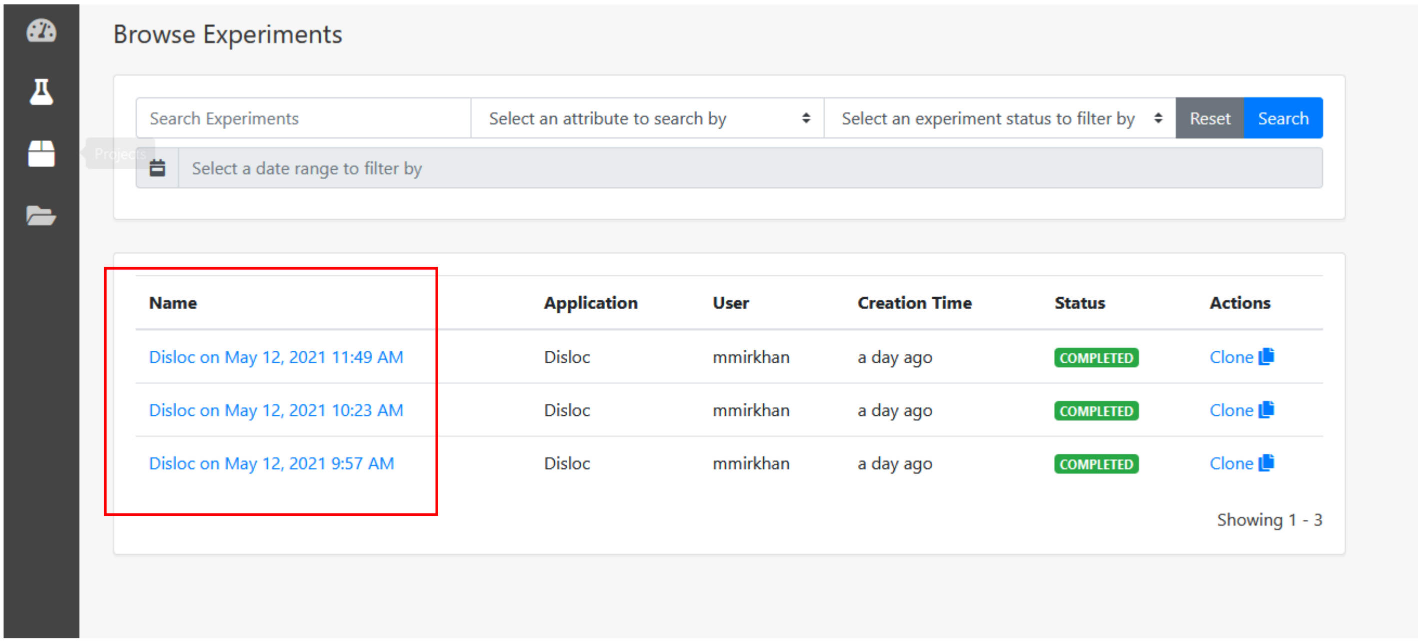

In the image below, the experiment summary and output files are displayed. Now, users may download each of these files.

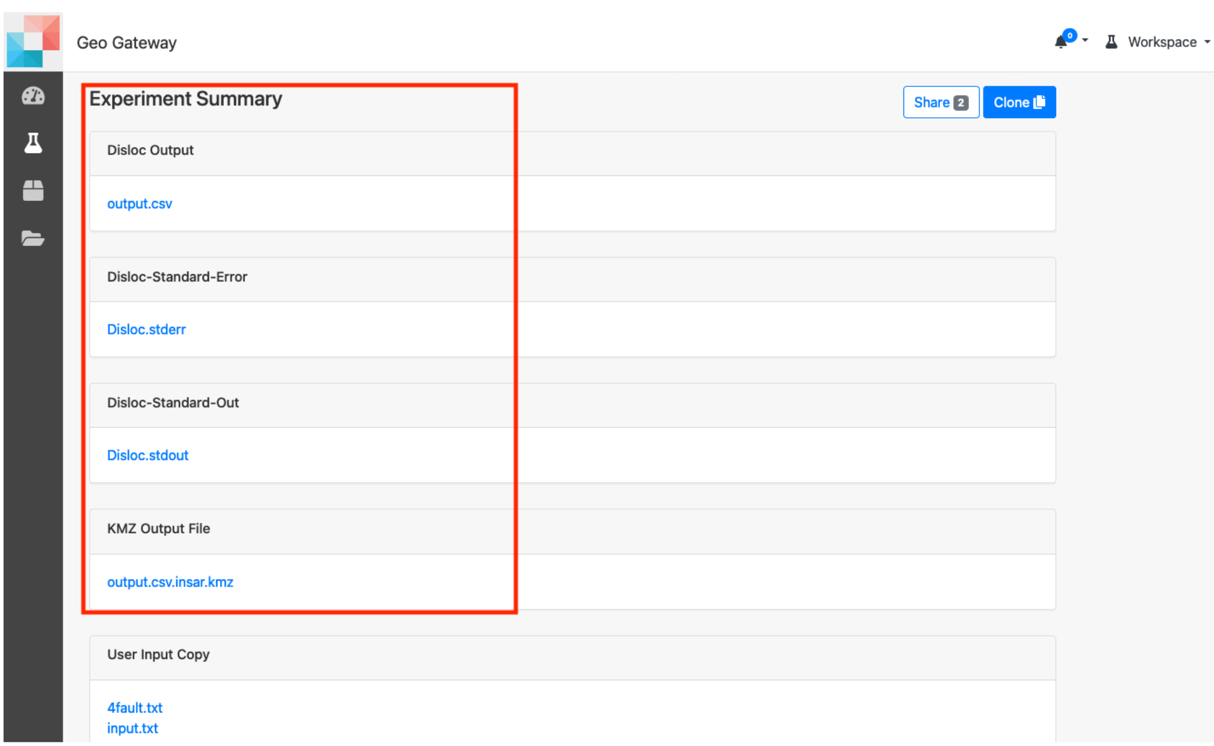

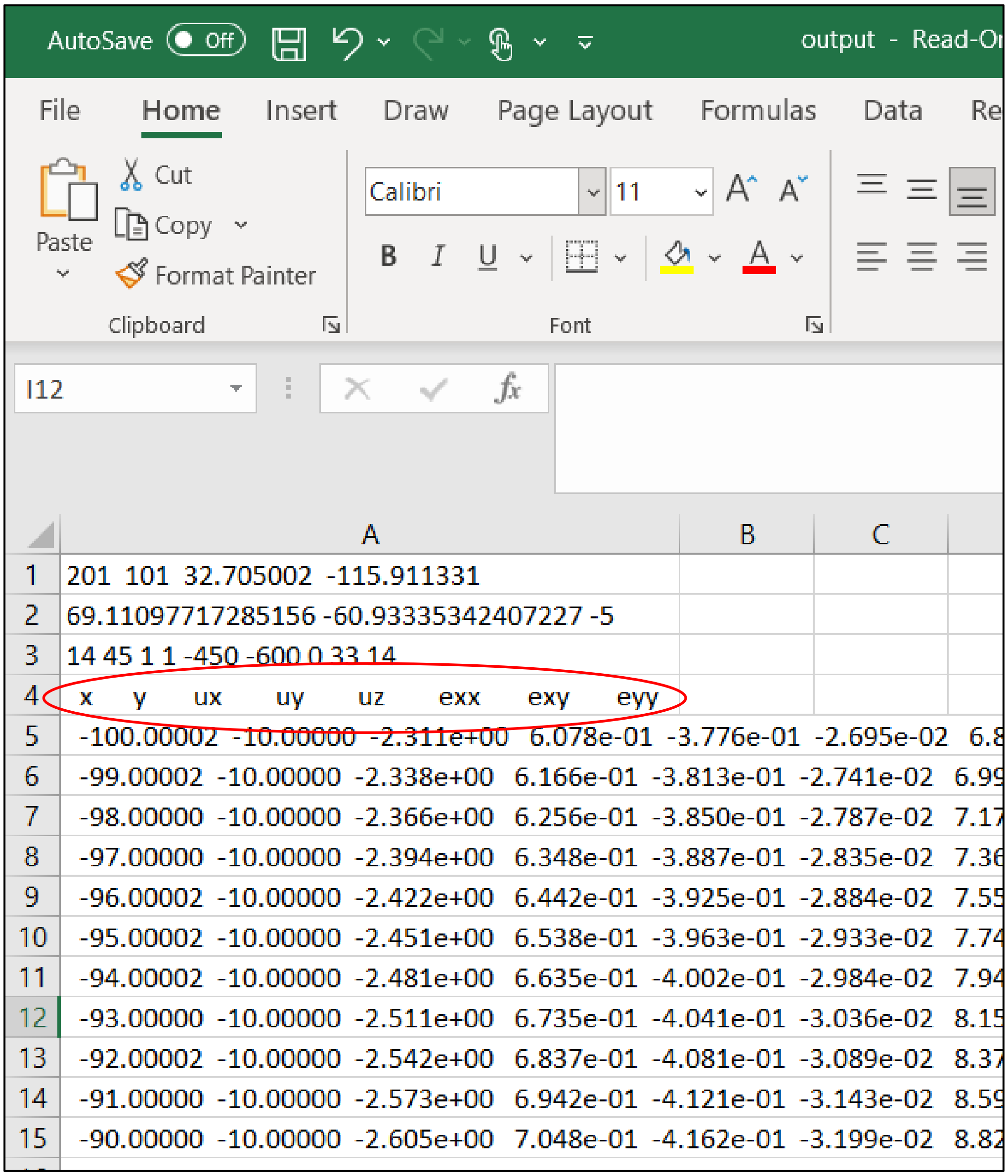

1	201 101 32.705002 -115.911331
2	69.11097717285156 -60.93335342407227 -5
3	14 45 1 1 -450 -600 0 33 14
4	x y ux uy uz exx exy eyy
5	-100.00002 -10.00000 -2.311e+00 6.078e-01 -3.776e-01 -2.695e-02 6.8
6	-99.00002 -10.00000 -2.338e+00 6.166e-01 -3.813e-01 -2.741e-02 6.99
7	-98.00000 -10.00000 -2.366e+00 6.256e-01 -3.850e-01 -2.787e-02 7.17
8	-97.00000 -10.00000 -2.394e+00 6.348e-01 -3.887e-01 -2.835e-02 7.36
9	-96.00002 -10.00000 -2.422e+00 6.442e-01 -3.925e-01 -2.884e-02 7.55
10	-95.00002 -10.00000 -2.451e+00 6.538e-01 -3.963e-01 -2.933e-02 7.74
11	-94.00002 -10.00000 -2.481e+00 6.635e-01 -4.002e-01 -2.984e-02 7.94
12	-93.00000 -10.00000 -2.511e+00 6.735e-01 -4.041e-01 -3.036e-02 8.15
13	-92.00002 -10.00000 -2.542e+00 6.837e-01 -4.081e-01 -3.089e-02 8.37
14	-91.00000 -10.00000 -2.573e+00 6.942e-01 -4.121e-01 -3.143e-02 8.59
15	-90.00000 -10.00000 -2.605e+00 7.048e-01 -4.162e-01 -3.199e-02 8.82

Figure 3: output.csv

Figure 3 displays the output.csv file which shows the x, y, U_1, U_2, and U_3 (refer to *figure 2*), and exx, exy, and eyy (components of the surface strain) factors. For more information regarding the parameters used please refer to (Okada, 1985).

Referring to Step 5, users must upload a text file. The figure below shows what the text file must include.

Line 1: Latitude Longitude # (The latitude and longitude are the model origin location, corresponding to x = 0, y = 0. The # represents the generation parameter. This tells how you will specify the points at which you want calculated displacements. If it is 0, this means you will be giving it a list of arbitrary x, y points (good for irregularly distributed sites). If it is 1, this means you are asking for output at regularly spaced points on a rectangular grid

Example of line 1: 32.705000 -115.911333 1

Line 2: x_0 x_Δ $x_\#$ y_0 y_Δ $y_\#$ (Represents the grid: This consists of starting x-coordinate (km), increment in x-direction (km), number of steps in x-direction, starting y-coordinate (km), increment in y-direction (km), number of steps in y-direction).

Example of line 2: -100 1 201 -10 1 101

Line 3: x, y (km) from origin and strike (degrees) (x coordinate and y coordinate of the first fault and the strike angle of the fault, measured clockwise from north)

Example of line 3: 69.110979 -60.933355 -5

Line 4: fault type 0 for point dislocation and 1 for rectangular plane dislocation, depth, dip (degrees), lambda (λ), mu (μ), u_1, u_2, u_3, length (km), width (km)

(Provide the vertical depth to the *bottom* of the fault, followed by the dip angle in degrees (zero for horizontal; 90° for vertical). The λ and μ are the Lamé elastic parameters, their absolute values are not important, only their ratio. For both lambda and mu, units are nominally Pascals (Pa), but in disloc, only their ratio is used, therefore the units cancel out. It is practical to set both to the value "1". Disloc then models the earth as an isotropic elastic solid with a Poisson Ratio of 0.25. λ=μ is the most common assumption for typical rocks. U_1, U_2, and U_3 are the amounts of relative slip to apply to the fault surface in the strike-slip, dip-slip, and tensile directions, respectively. Positive U_1 corresponds to *left-lateral motion* (opposite in sense to the San Andreas fault for example. Positive U_2 corresponds to *thrusting motion* with the hanging wall riding up over the foot wall (like the San Gabriel mountains for example). U_3 will not normally be used since ordinary earthquake faults involve motion only tangential to the fault plane. Finally, the length and width of the rectangular fault surface.)

Example of line 4: 1 14 45 1 1 -450 -600 0 33 14

Repeat the formatting from line 3 and line 4 for each additional fault.

Example of line 5 (same format as line 3): 56.877979 -45.030355 -48

Example of line 6 (same format as line 4): 1 15 75 1 1 -830 0 0 51 15

Example of line 7 (same format as line 3): 46.475979 -56.538355 132

Example of line 8 (same format as line 4): 1 14 60 1 1 -830 0 0 60 14

Example of line 9 (same format as line 3): 25.940979 -9.411355 -25

Example of line 10 (same format as line 4): 1 12 50 1 1 -100 0 0 18 12

To view the output files on the map

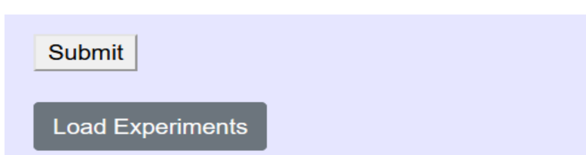

To allow the output file to be shown on GeoGateway, return to the Disloc tab on the GeoGateway website and click on "Load Experiments" as shown in the image below. Once the experiments appear, click on the green highlighted text

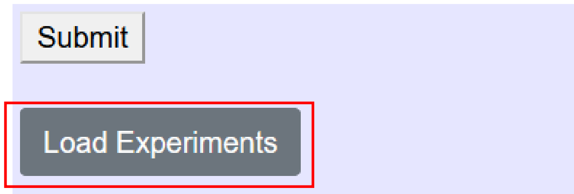

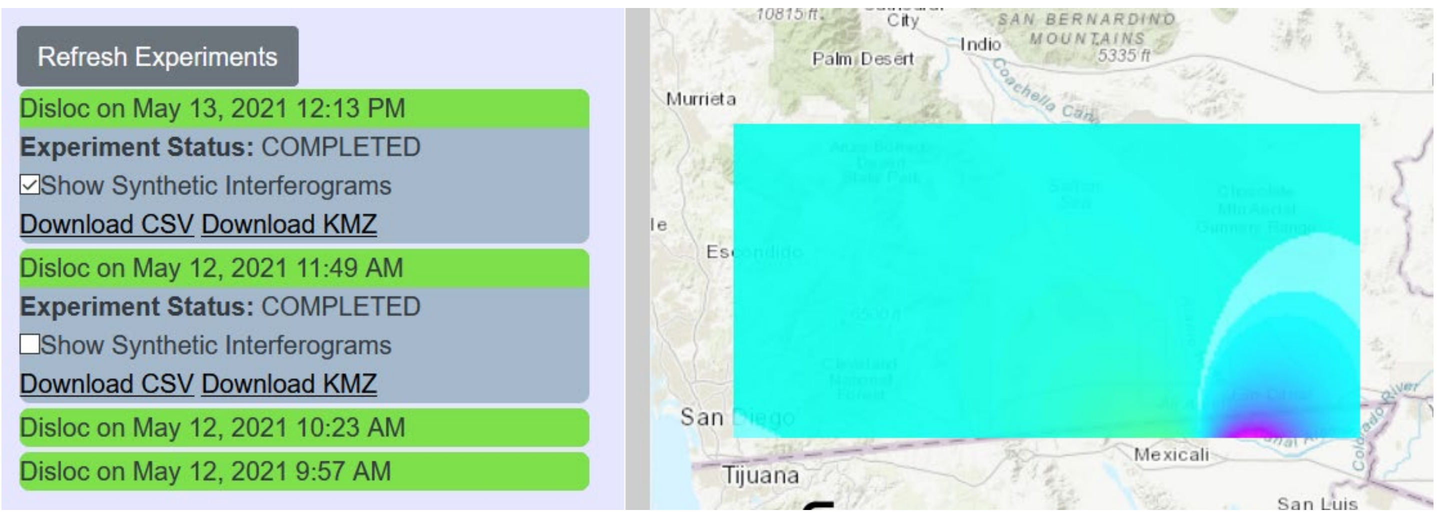

Figure 5: Dislocation output data displayed on map on GeoGateway. The image is in correspondence to lines 1-4 from figure 4.

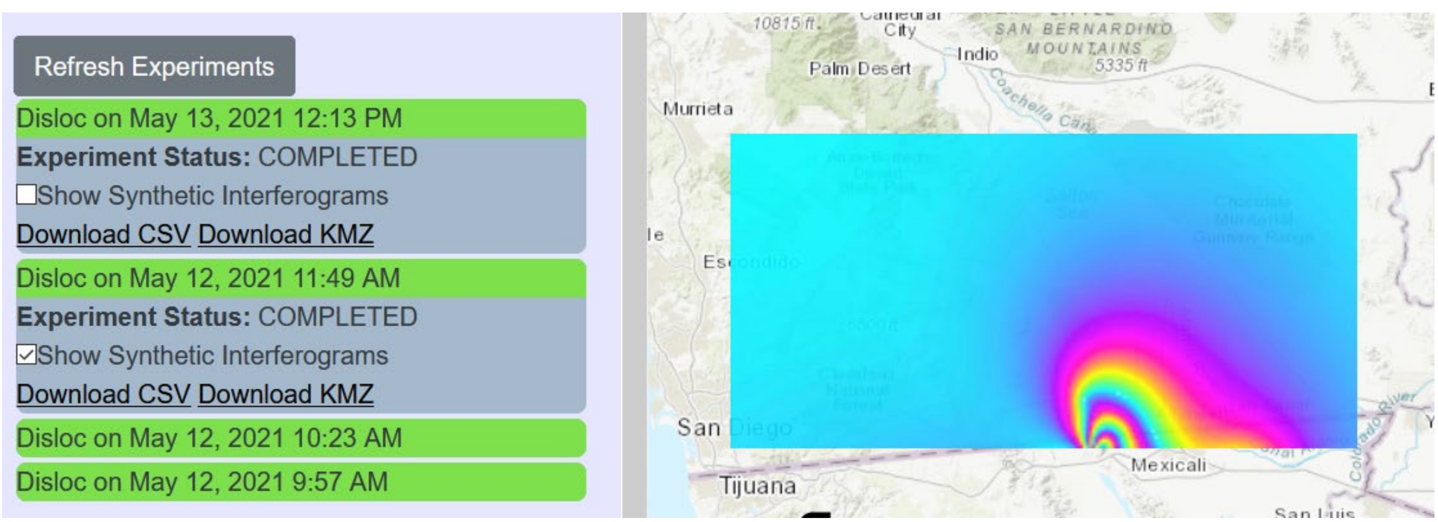

Figure 6: Dislocation output data displayed on map on GeoGateway. The image is in correspondence to lines 1-10 from figure 4.

Special Studies

GeoGateway's Special Studies tab lists products for demonstration purposes. The study includes wildfire burn areas and debris flows imaged with UAVSAR following the Southern California 2018 Woolsey Fire shown in figure (2) below; and the 2017 Montecito, California fire, in figure (4) below. See *Donnellan et al. 2018* for more information on the Montecito, CA fire.

Figure 1: Woolsey Fire (figure adapted from courtesy of Wally Skalij from the Los Angeles Times)

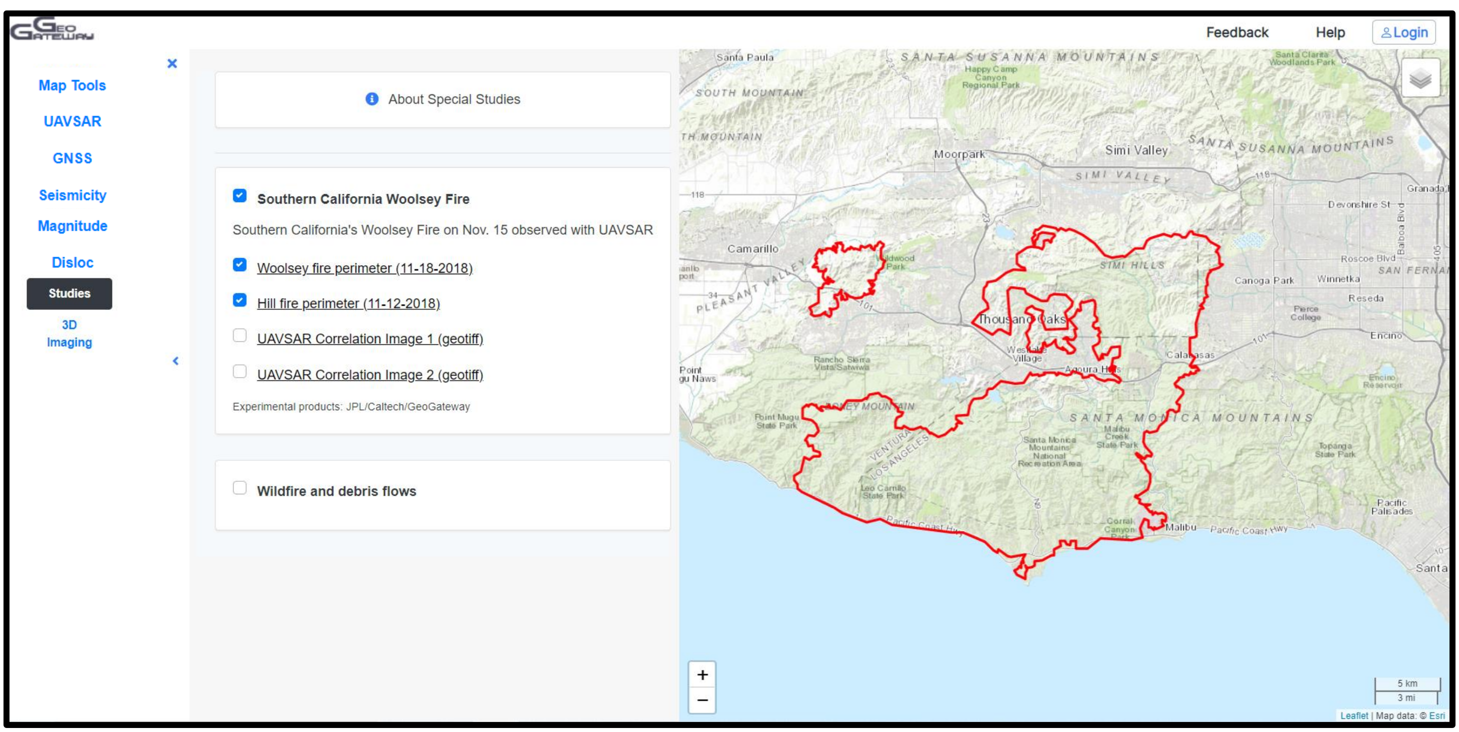

Figure 2(a): Woolsey Fire and Hill fire perimeter

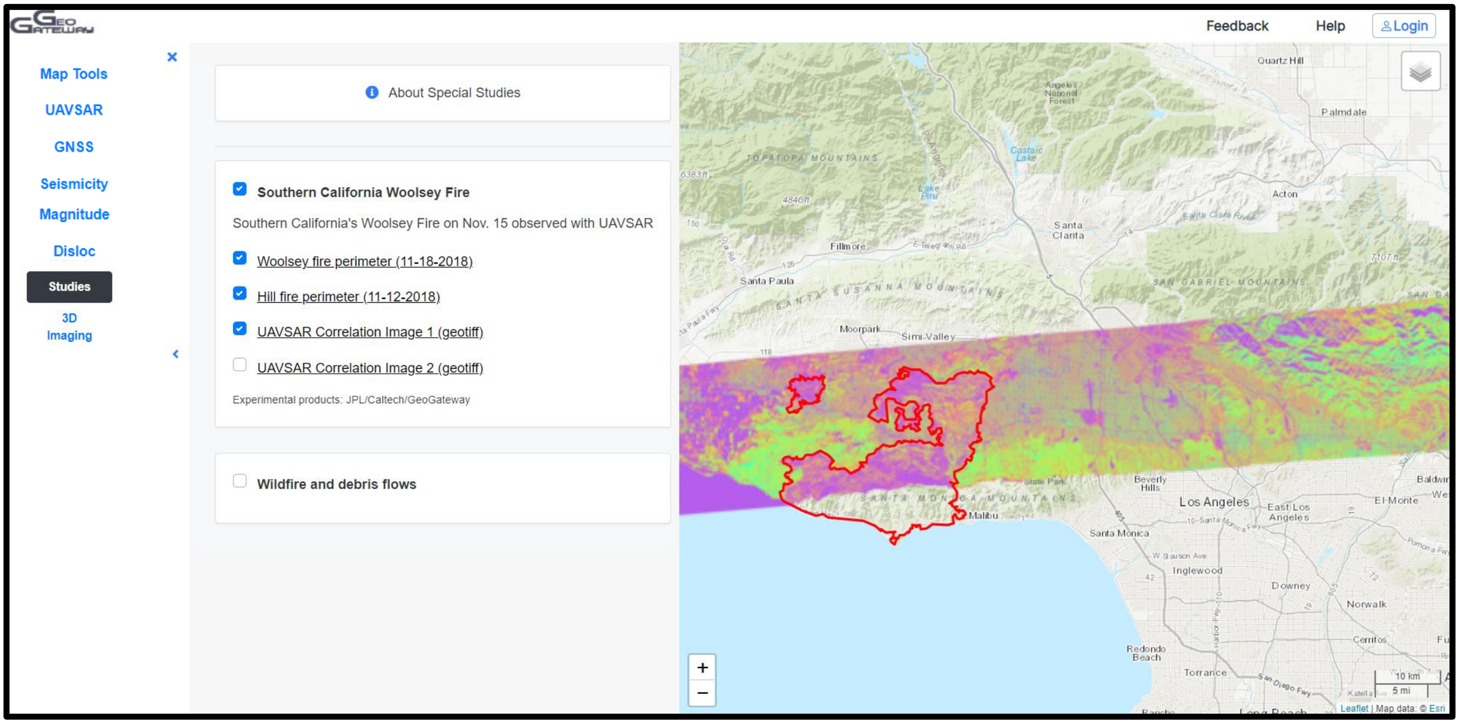

Figure 2(b): UAVSAR correlation image (1) of Woolsey fire. UAVSAR can see through smoke, clouds, and the dark of night.

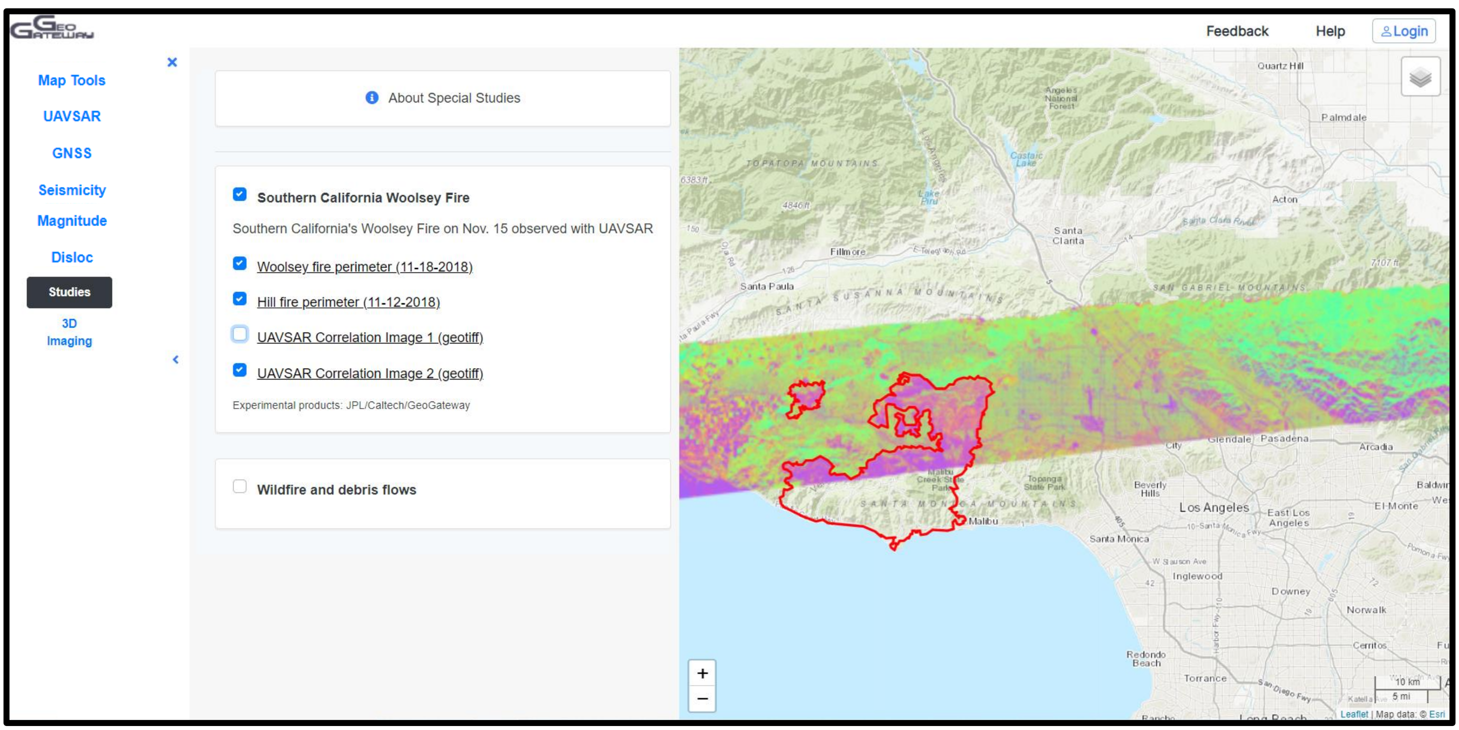

Figure 2(c): UAVSAR correlation image (2) of Woolsey fire.

Figure 3: Debris flow on Highway 101 following the Thomas Fire in Montecito (figure adapted from courtesy of Trevor Hughes, USA TODAY)

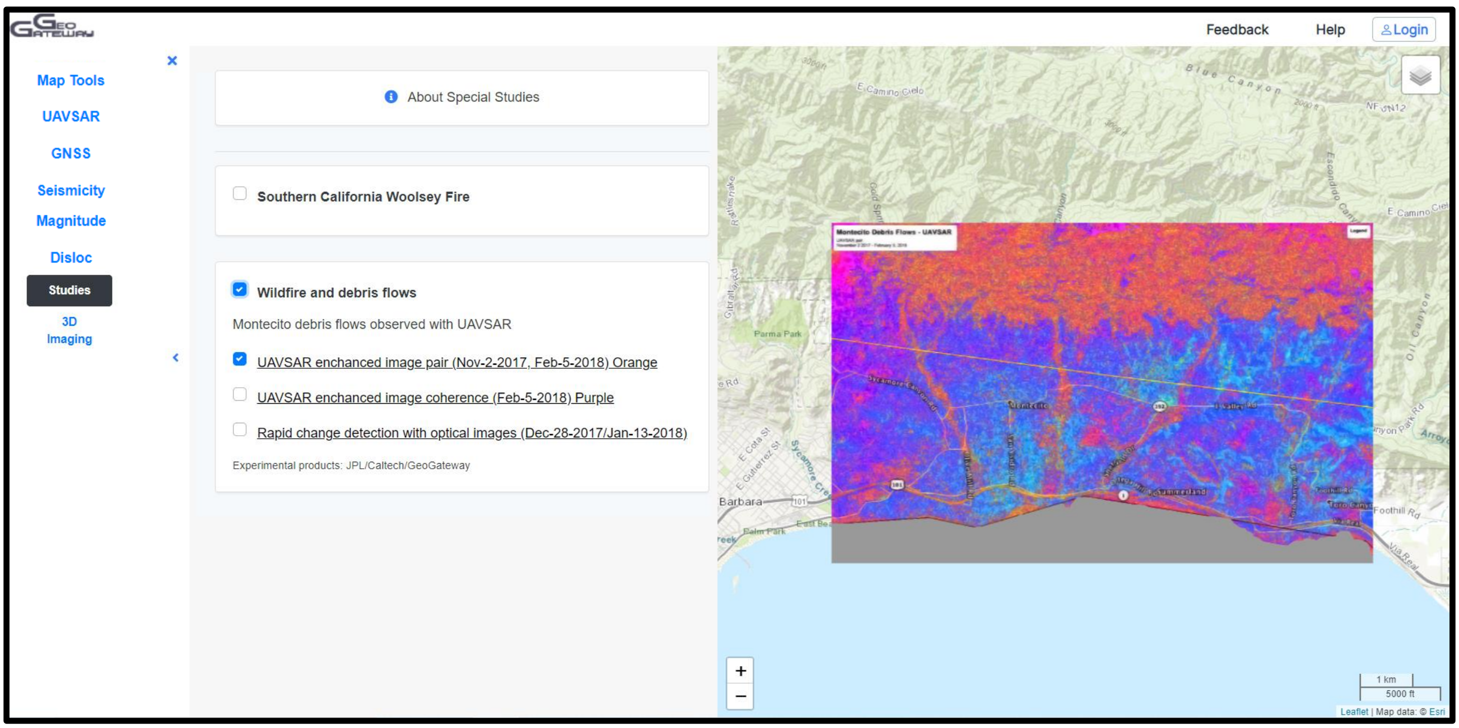

Figure 4(a): The image displays UAVSAR high-resolution interferogram that has been despeckled, converted to four colors and contrast increased. Orange represents the disturbed areas, and debris flows can be seen extending from the fire scar south of the outline.

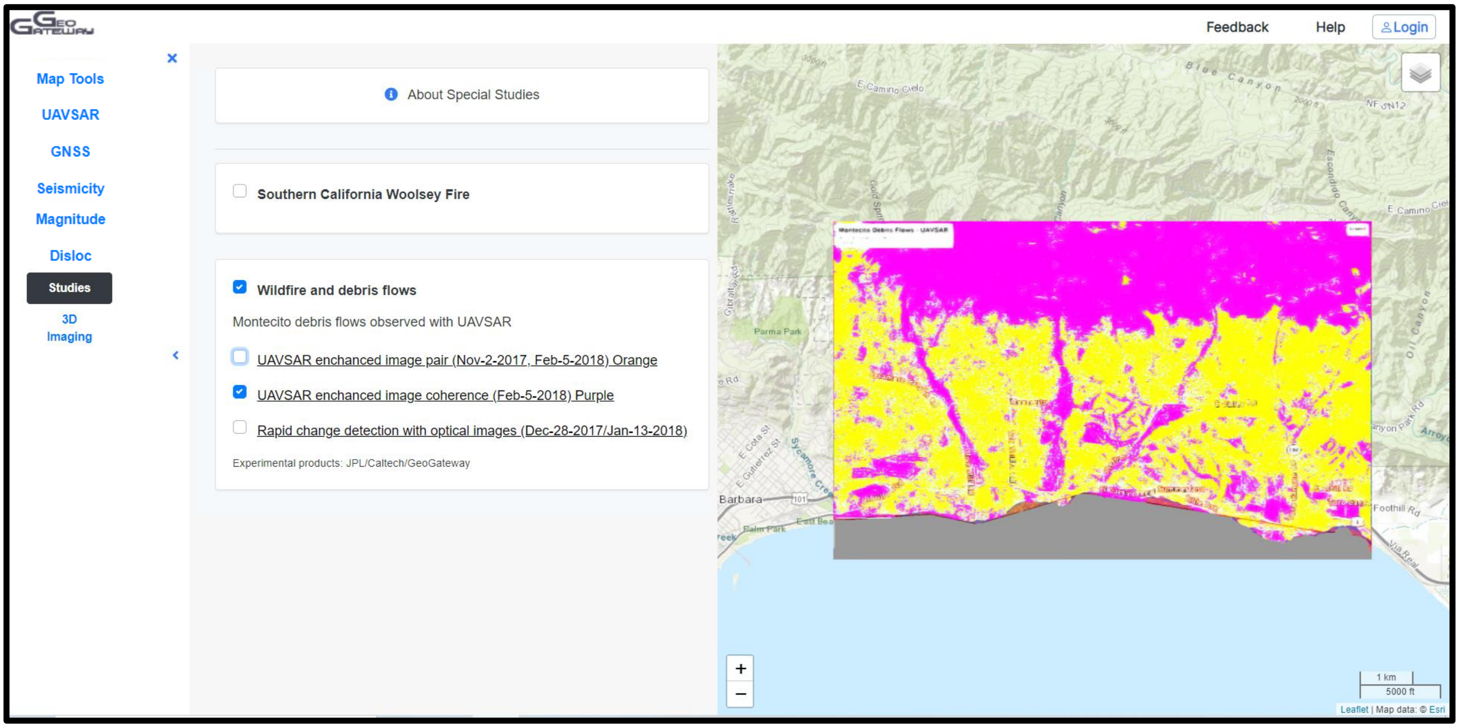

Figure 4(b): The image displays UAVSAR high-resolution correlation image that has been despeckled, converted to two colors and contrast increased. Purple represents the disturbed areas and are decorrelated, and debris flows can be seen extending from the fire scar.

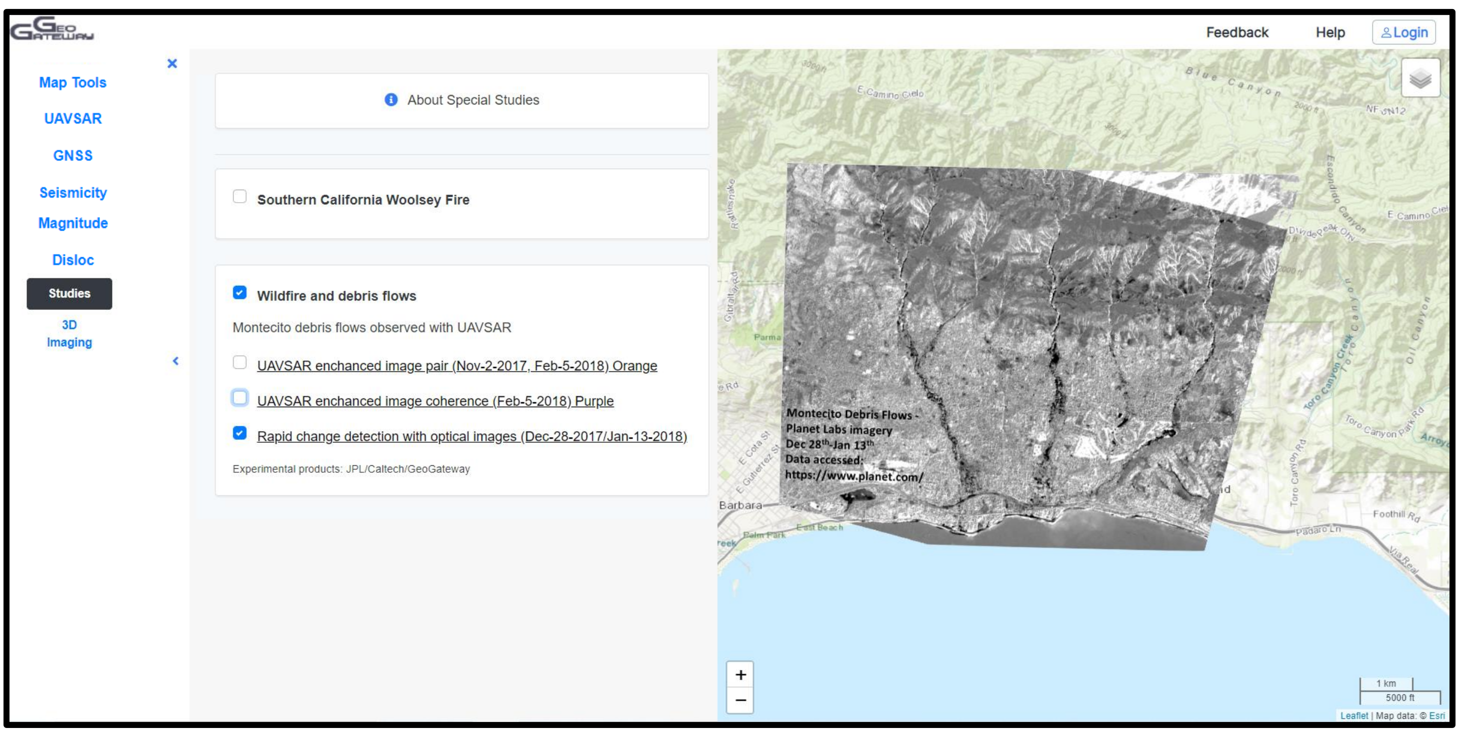

Figure 4(c): Montecito debris flow optical image.

3D Imaging

Figure 1: Earthquake Damage on California Hwy 178 figure adapted by (Ben Brooks, USGS)

Users can locate postseismic products of the Ridgecrest Earthquake (M6.4 (July 4, 2019) and M7.1 (July 5, 2019)) by navigating to the “3D Imaging” tab and clicking on the box labeled “Postseismic Products of Ridgecrest Earthquake.”

The data was collected by Andrea Donnellan and Gregory Lyzenga.

More information regarding the data can be obtained by clicking on the citation below

[Andrea Donnellan, Gregory Lyzenga, Adnan Ansar, Christine Goulet, Jun Wang, Marlon Pierce; Targeted High-Resolution Structure from Motion Observations over the MwMw 6.4 and 7.1 Ruptures of the Ridgecrest Earthquake Sequence. Seismological Research Letters doi: https://doi.org/10.1785/0220190274]

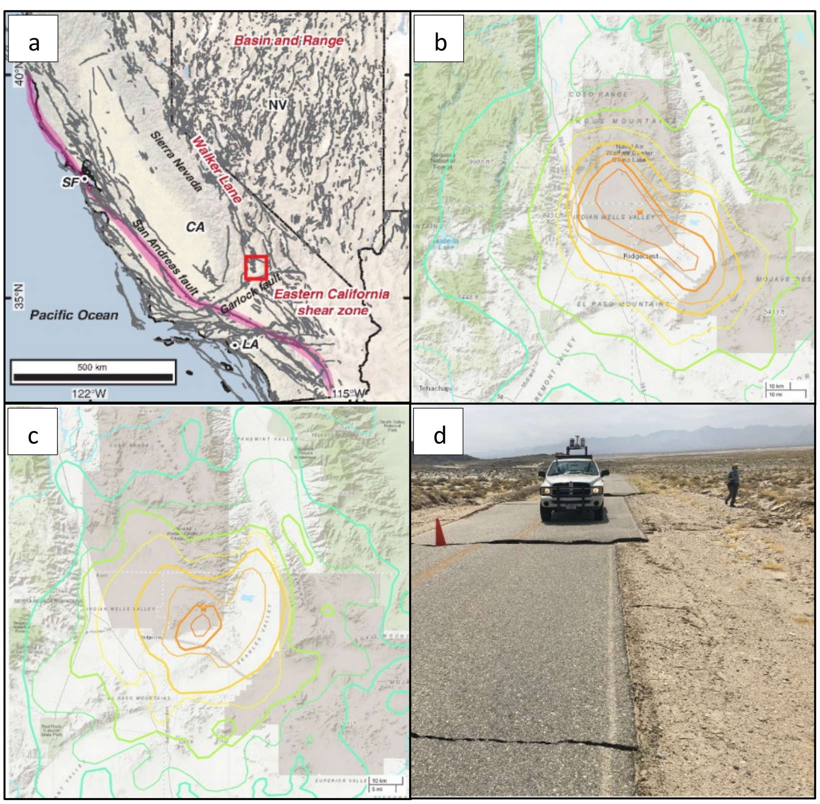

Figure 2: Figures from 2019 Ridgecrest earthquake

2(a) Boxed location shows location of the Ridgecrest earthquakes. Picture adapted from (Jobe et al., 2020)

2(b) Shaking intensity levels associated with each contour color shown for Mw 7.1 earthquake event. Warm colors represent higher intensity and color colors represent lower intensity. Picture adapted from (USGS, 2020).

2(c) Shaking intensity levels associated with each contour color shown for Mw 6.4 earthquake event. Warm colors represent higher intensity and color colors represent lower intensity. Picture adapted from (USGS, 2020).

2(d) Road offset on the road at Naval Air Weapons Station China Lake (NAWSCL) from the M7.1 rupture (Ben Brooks, USGS).

The products included in the 3D Imaging tab comprise of,

1. **Inferred rupture traces and orthomosaic images** for the M6.4 earthquake and M7.1 earthquake, which can be selected by clicking on the corresponding box. The inferred rupture traces can be downloaded as a KML.
2. Six **point cloud** (in LAZ format), which can be downloaded for each earthquake by clicking on “Point Cloud” across the listed dates which range from 2019/07/09 to 2019/09/27. Further, clicking on the “2cm DSM” option will download a 2 cm Digital Surface Model (in LAZ format). A quality report can be accessed by clicking on “Report.”
3. **Digital Surface Model (DSM) and orthomosaic image** ,which can be downloaded as a KMZ by clicking on “Products overview (kmz).”
4. **Data from Potee**, a viewer for large point cloud/LIDAR data sets, which can be accessed and viewed by clicking on "View Point Clouds.” Potree allows for users to adjust the appearance, clip, measure, export, and complete several other actions to the orthomosaic images.
5. An **animated GIF** of the M7.1 earthquake, which can be accessed by clicking on the “Animated Gif” button under M7.1 products.

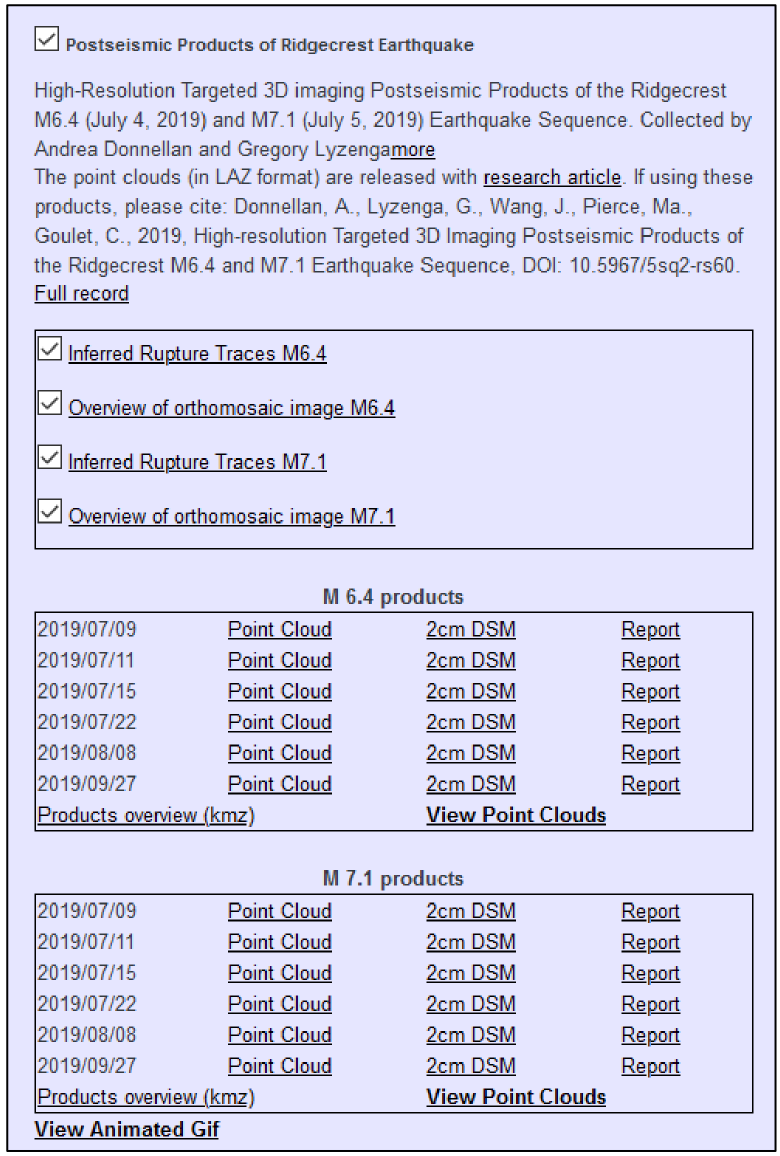

Figure 3: 3D Imaging tab content

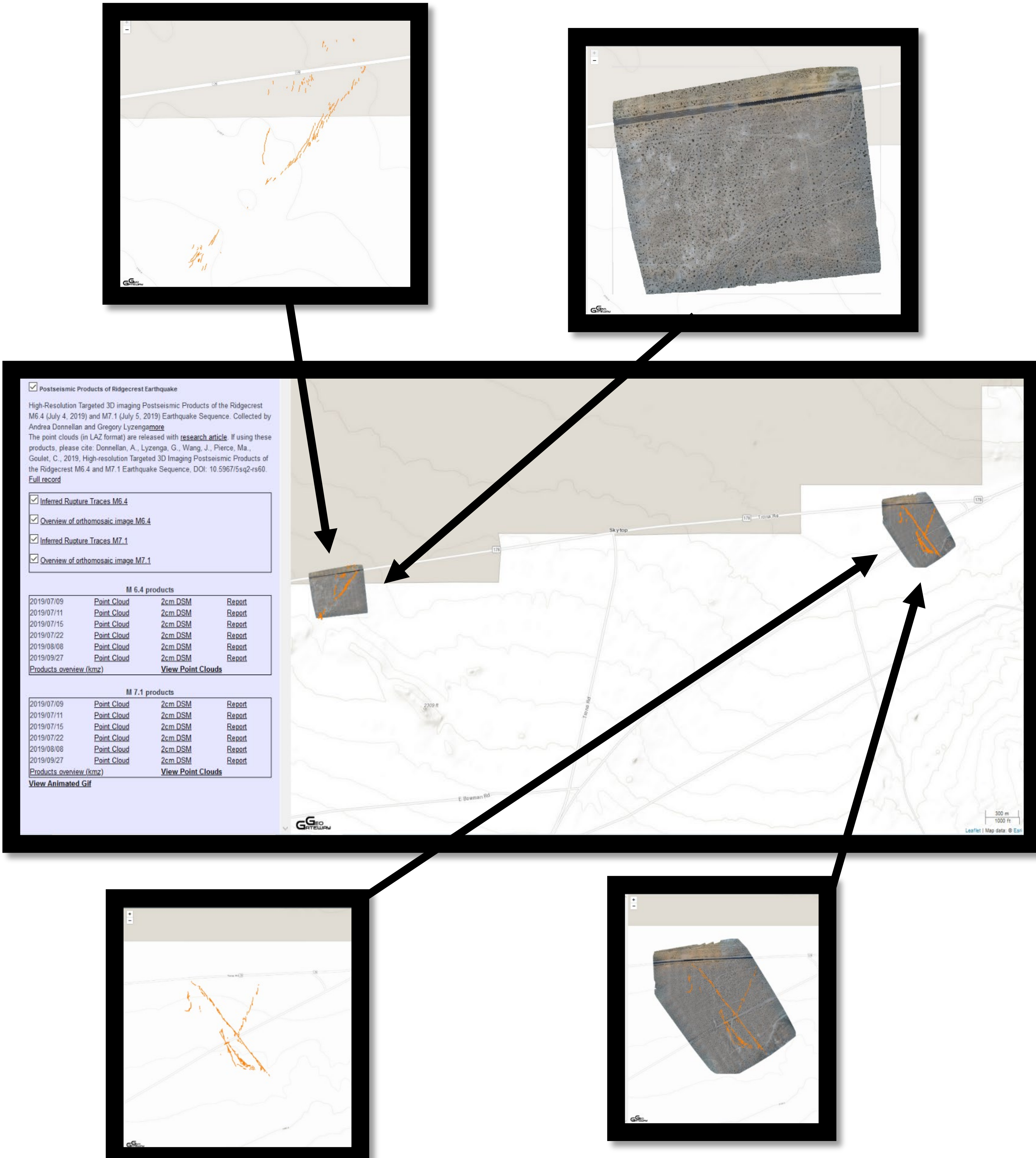

Postseismic Products of Ridgecrest Earthquake
High-Resolution Targeted 3D imaging Postseismic Products of the Ridgecrest M6.4 (July 4, 2019) and M7.1 (July 5, 2019) Earthquake Sequence. Collected by Andrea Donnellan and Gregory Lyzengamore
The point clouds (in LAZ format) are released with research article. If using these products, please cite: Donnellan, A., Lyzenga, G., Wang, J., Pierce, Ma., Goulet, C., 2019, High-resolution Targeted 3D Imaging Postseismic Products of the Ridgecrest M6.4 and M7.1 Earthquake Sequence, DOI: 10.5967/5sq2-rs60.
Full record
Inferred Rupture Traces M6.4
Overview of orthomosaic image M6.4
Inferred Rupture Traces M7.1
Overview of orthomosaic image M7.1
M 6.4 products
2019/07/09 Point Cloud 2cm DSM Report
2019/07/11 Point Cloud 2cm DSM Report
2019/07/15 Point Cloud 2cm DSM Report
2019/07/22 Point Cloud 2cm DSM Report
2019/08/08 Point Cloud 2cm DSM Report
2019/09/27 Point Cloud 2cm DSM Report
Products overview (kmz)
View Point Clouds
M 7.1 products
2019/07/09 Point Cloud 2cm DSM Report
2019/07/11 Point Cloud 2cm DSM Report
2019/07/15 Point Cloud 2cm DSM Report
2019/07/22 Point Cloud 2cm DSM Report
2019/08/08 Point Cloud 2cm DSM Report
2019/09/27 Point Cloud 2cm DSM Report
Products overview (kmz)
View Point Clouds
View Animated Gif

References:

Avouac, J.-P. (n.d.). Appendix: On the use of the 'Elastic Dislocations.' ftp://ftp.gps.caltech.edu/pub/avouac/Ge177/Presentations-old/(10) Appendix_Elastic Dislocation.ppt

Britannica. (n.d.). Longitude geography. https://www.britannica.com/science/longitude

Chen, J., Tang, H., & Chen, W. (2020). Deep learning of the aftershock hysteresis effect based on the elastic dislocation theory. Natural Hazards and Earth System Sciences, 20(11), 3117–3134. https://doi.org/10.5194/nhess-20-3117-2020

Donnellan, A., Parker, J., Heflin, M., Glasscoe, M., Lyzenga, G., Pierce, M., Wang, J., Rundle, J., Ludwig, L. G., Granat, R., Mirkhanian, M., & Pulver, N. (2021). Improving access to geodetic imaging crustal deformation data using GeoGateway. Earth Science Informatics. https://doi.org/10.1007/s12145-020-00561-7

Donnellan, A., Parker, J., Hensley, S., Pierce, M., Wang, J., & Rundle, J. (2014). UAVSAR observations of triggered slip on the Imperial, Superstition Hills, and East Elmore Ranch Faults associated with the 2010 M 7.2 El Mayor-Cucapah earthquake. AGU: Geochemistry, Geophysics, Geosystems, 815–829. https://doi.org/10.1002/ 2013GC005120

Donnellan, A., Parker, J., Milliner, C., Farr, T. G., Glasscoe, M., Lou, Y., Zheng, Y., & Hawkins, B. (2018). UAVSAR and Optical Analysis of the Thomas Fire Scar and Montecito Debris Flows: Case Study of Methods for Disaster Response Using Remote Sensing Products. Earth and Space Science, 5(7), 339–347. https://doi.org/10.1029/2018EA000398

Harvey Mudd College. (n.d.). Elastic Dislocation Fault Parameters. 1–2. http://www.physics.hmc.edu/GL/misc/disloc.pdf

Heflin, M., Donnellan, A., Parker, J., Lyzenga, G., Moore, A., Ludwig, L. G., et al. (2020). Automated estimation and tools to extract positions, velocities, breaks, and seasonal terms from daily GNSS measurements: illuminating nonlinear Salton Trough deformation. Earth and Space Science, 7, e2019EA000644. https://doi.org/10.1029/2019EA000644

Incorporated Research Institutions for Seismology (IRIS). (n.d.) How Often Do Earthquakes Occur? IRIS - Education and Outreach Series, 3. https://www.iris.edu/hq/inclass/fact-ss qqsheet/how_often_do_earthquakes_occur

Jet Propulsion Laboratory. (2014). What is UAVSAR? https://uavsar.jpl.nasa.gov/education/what-is-uavsar.html

Jobe, J. A. T., Philibosian, B., Chupik, C., Dawson, T., Bennett, S. E. K., Gold, R., DuRoss, C., Ladinsky, T., Kendrick, K., Haddon, E., Pierce, I., Swanson, B., & Seitz, G. (2020). Evidence of Previous Faulting along the 2019 Ridgecrest, California, Earthquake Ruptures. Bulletin of the Seismological Society of America. https://doi.org/https://doi.org/10.1785/0120200041

Okada, Y. (1985). Internal deformation due to shear and tensile faults in a half-space. Bulletin – Seismological Society of America, 82(2), 1018–1040. https://watermark.silverchair.com/BSSA0750041135.pdf?token=AQECAHi208BE49Ooan9kkhW_Ercy7Dm3ZL_9Cf3qfKAc485ysgAAAvowggL2BgkqhkiG9w0BBwagggLnMIIC4wIBADCCAtwGCSqGSIb3DQEHATAeBglghkgBZQMEAS4wEQQM0wXyjLzqC9G7ZjvwAgEQgIICrT9Ww8cdmlGOvsTkX_vITtpWyJGHuXAYQkjyJqRA

Other Global Navigation Satellite Systems (GNSS). (2020). The Global Positioning System. https://www.gps.gov/systems/gnss/

Parker, J., Donnellan, A. and Glasscoe, M.T. (2021). Survey of Transverse Range Fire Scars in Ten Years of UAVSAR Polarimetry. Earth and Space Science, 8, e2021EA001644. https://doi.org/10.1029/2021EA001644.

UNAVCO. (2020). Network of the Americas (NOTA). https://www.unavco.org/projects/major-projects/nota/nota.html

USGS. (n.d.). About GPS. https://earthquake.usgs.gov/monitoring/gps/about.php

USGS. (2021). USGS Magnitude 2.5+ Earthquakes, Past Day. https://earthquake.usgs.gov/earthquakes/map/?extent=23.64452,-125.46387&extent=50.6808,-64.51172

Vista Heights Middle School. (n.d.). Modeling the Calculation of an Earthquakes Seismic Moment. https://vhmsscience.weebly.com/seismic-moment-model.html